SafeWind

Collaborative project funded by the European Commission under the 7th Framework Program, Theme 2007-2.3.2: Energy

"Multi-scale data assimilation, advanced wind modelling & forecasting with emphasis to extreme weather situations for a safe large-scale wind power integration"

Grant Agreement N°: 213740

# DELIVERABLE Dp-4.2

# "Impact of data assimilation for shortest-term Wind Power Forecasting (WPF)"

| | |
|---|---|
| DOCUMENT TYPE | Deliverable |
| DOCUMENT NAME: | swind.deliverable_Dp-4.2_v1.0 |
| VERSION: | V1.0(*) |
| DATE: | 30 October 2012 |
| CLASSIFICATION: | R0:General Public |
| STATUS: | S0: Approved |

**Abstract:**
With increasing shares of wind power, the prediction of wind power must be continuously improved on almost all time scales to facilitate the integration of variable wind power. Work package 4 of the SafeWind project focuses on the shortest-term forecast range (0-6 h) and investigates the use of new methods and/or new and existing data sources to provide near real-time updates of the "wind energy weather". In Task 4.2 "Data assimilation based on observations and detection of large forecast deviations due to extreme events" the partners UNIOL and DTU.RISOE investigated the potential of data assimilation with the mesoscale WRF (Weather and Research Forecasting) model in two different case studies.
DTU.RISOE utilizes the offshore wind park Horns Rev I as a test bed to assimilate wind speeds from up to 80 nacelle anemometers into WRF. The results clearly indicate that Four-Dimensional Data Assimilation (FDDA) improves shortest-term forecasts. After a forecast horizon of about 2 h the assimilated information is advected downstream and does not affect the wind farm anymore.
UNIOL has applied FDDA and 3dVar for a domain over the North Sea. About 470 synop, buoys and air craft reports plus about 20 vertical soundings have been assimilated per hour during the study period of 1-30 April 2008. ECMWF and NCEP short-term forecast runs have been used as initial and boundary conditions. The verification with FINO1 100m wind speeds shows clearly that FDDA matches the measurement better than 3dVar. In the best case, WRF FDDA lowered the initial RMSE from 1.75 m/s to 1.45 m/s for ECMWF and from 2.05 m/s to 1.65 m/s for NCEP.

| AUTHORS[1], REVIEWERS | | | | |
|---|---|---|---|---|
| MAIN AUTHOR/EDITOR: | Lueder von Bremen | | | |
| AFFILIATION: | University of Oldenburg (UNIOL) | | | |
| ADDRESS: | ForWind, Ammerländer Heerstr.136, 26129 Oldenburg, Germany | | | |
| TEL.: | +49 441 798 5071 | | | |
| EMAIL: | Lueder.von.bremen@forwind.de | | | |
| FURTHER AUTHORS: | Caroline Draxl (Risoe, now NCAR), J. Jiang (UNIOL, now Desert Research Institut, Nevada) | | | |
| PEER REVIEWERS: | Constantin Junk (UNIOL) | | | |
| REVIEW APPROVAL: | 30 October 2012 | L. von Bremen | Approved | |
| SUGGESTED IMPROVEMENTS: | *For a long list of remarks make reference to another document* | | | |

| VERSION HISTORY | | | |
|---|---|---|---|
| VERSION[2]: | DATE: | COMMENTS, CHANGES, STATUS: | PERSON(S): |
| 0.1 | 21.02.2011 | Initial version | Lueder von Bremen |
| 0.1 | Feb 2012 | Caroline inserted her part | Caroline Draxl |
| 0.2 | 26.06.2012 | Editorial changes and remarks to Carolines part | Lueder von Bremen |
| 0.4 | 23.07.2012 | Version for review | Lueder von Bremen |
| 1.0 | 30.10.2012 | Approved version after review | Lueder von Bremen |
| | | | |

| STATUS, CONFIDENTIALITY, ACCESSIBILITY | | | | | | | | | |
|---|---|---|---|---|---|---|---|---|---|
| STATUS: | | | | CONFIDENTIALITY: | | | | ACCESSIBILITY: | |
| **S0** | Approved/Released | X | | **R0** | General public | X | | Private web site | |
| **S1** | Reviewed | | | **R1** | Restricted to project members | | | Public web site | X |
| **S2** | Pending for review | | | **R2** | Restricted to European Commission | | | Paper copy | |
| **S3** | Draft for comments | | | **R3** | Restricted to WP members + PL | | | | |
| **S4** | Under preparation | | | **R4** | Restricted to Task members +WPL+PL | | | | |

**PL:** *Project leader* **WPL:** *Work package leader* **TL:** *Task leader*

1 **The authors of this document are solely responsible for its content, which does not represent the opinion of the European Community and the European Community is not responsible for any use that might be made of data appearing therein.**

2 **VERSION NAMING : V0.x** draft before peer-review approval, **V1.0** at the approval, **V1.x** minor revisions, **V2.0** major revision

# Contents

# 1. Introduction

The ambitious plans for offshore wind power deployment are a financial and technical challenge with respect to the safe integration into the power supply system. Without any doubt the integration is technical feasible but it is necessary that the amounts of reserve power (most likely by conventional power plants) can be justified with respects to the economics of wind power. In that sense, a high concentration of offshore wind power, for example in the German Bight, is highly vulnerable to weather related errors in short and shortest-term wind power forecasts.

To achieve stable and reliable operation of an electrical power system, the system operator must actively maintain a balance between supply and demand of power at any point in time. Unlike conventional power plants, the power output of wind turbines is subject to strong fluctuations due to the variability of wind, which makes its integration into the grid challenging. Balancing the grid is a process spanning several timescales, and not all energy resources possess the same amount of flexibility for contributing to it. Depending on the technology, a cold start of a power plant may take several hours or even a full day. Rapid changes in power output may be impossible or cost inefficient for some units. To ensure a balanced power system, the use and operation of the different resources has to be scheduled in advance. Power system operation always includes elements of uncertainty: the amount of energy consumption cannot be exactly determined ahead of time, and equipment failure can lead to sudden loss of generation or consumption. Reserve capacity has to be allocated to account for this uncertainty. The introduction of wind power increases the need for these reserves because of its natural variability. Wind forecasts are a key element to reduce and account for the uncertainty associated with this variability. Resource allocation occurs on several time scales. Wind power producers commit to the delivery of a certain amount of energy on a day-ahead market. Foreseeable deviations from their commitment can be settled on an intra-day market up to one hour before delivery, usually at a higher price. Mismatch between contractual and actual production within the operating hour is then handled by the system operator through the deployment of regulating reserves. The high cost of deploying these reserves is paid by the power producer, who is obliged to settle the mismatch by buying so-called balancing power from the system operator. Trading the power on energy markets is particularly important in countries where the produced wind power has to be fed into the grid by law, like in Denmark; but also in countries with an optional integration of produced wind power, e.g., in the USA, there are incentives to use wind forecasts to determine operating reserve requirements [Botterud et al, 2009] or to trade the power on energy markets [Botterud et al, 2010], [Marquis et al, 2011].

As a consequence to rapidly increasing shares of wind power, the prediction of wind power must be continuously improved on almost all time scales to facilitate the integration of variable wind power.

Work package 4 of the SafeWind project focuses on the shortest-term forecast range (0-6 hours) and investigates the use of new methods and/or new and existing data sources to provide near real-time updates of the “wind energy weather”. Updates of wind power forecasts are of high importance to grid operators to activate reserves in case high deviations to previously forecasted wind power are likely to occur. Furthermore, wind park operators that sold their wind energy at the power market and are thus likely to fall short, have a high interest to buy balancing energy rather than to pay high penalties in case of non-fulfilment of their delivery contract.

The key to excellent shortest-term wind power forecasts is to incorporate latest measurements that contain direct or indirect information about the spatial and temporal evolution of wind power production up to the time of their observation. Direct observations correspond to wind power production data while indirect observations have to be converted into wind power before issuing updated wind power forecasts. However, the information content of wind power is limited whenever nominal power is reached or even cut-off wind speed are reached and the turbine is shut down.

It is straight forward to use upstream wind observations to spot upstream wind forecast errors. Assuming that the pattern of wind forecast errors does not change significantly with time, those upstream forecast errors propagate to the site of interest (Taylor hypothesis). A different approach for shortest-term wind power forecasting is to make use of the strong spatial correlation of wind and wind

power. Hence, it can be anticipated that if high wind power occurs upstream, the wind power will increase with a certain time delay at the site of interest. This methodology has been used by several authors. Wessel el al., 2009 and Larson and Westrick, 2006 gained little improvements in shortest-term wind power forecasts when upstream wind power observations served as additional input, besides NWP data, to statistical wind power prediction tools.

In Task 4.2 “Data assimilation based on observations and detection of large forecast deviations due to extreme events” the partners University Oldenburg and DTU.RISOE investigated the potential of data assimilation with the mesoscale WRF (Weather and Research Forecasting) model. In the case of DTU.RISOE nacelle wind speeds are used as a new data source. Data assimilation as applied in Numerical Weather Prediction (NWP) aims to update a given (model) state of the atmosphere (first guess) with (new) observations. Different approaches exist and two of them are described and applied in this report, namely Four-Dimensional Data Assimilation (FDDA) and three-dimensional variational (3dVar) data assimilation.

Data assimilation is a time critical application since the faster the updated state of the atmosphere (i.e. analysis) is available, the better for the following application or decision chain. Thus, a compromise has to be found with respect to computing time of complexity and skill of the chosen data assimilation approach. However, in this study no constraints are set with respect to timeliness of incoming observations or first guess data that is typically taken for short-range weather forecasts. This means, the conducted experiments in this study are not possible in an operational time-critical environment because certain input data would not be available in time. The study can be regarded as a feasibility study in an idealized environment to explore the potential of data assimilation for shortest-term wind power forecasting. The experience can be used to identify and formulate further research needs in the area of data assimilation and wind energy application, in particular in combination with new observation types, e.g. nacelle wind speeds.

# 2. Data assimilation with WRFvar

## 2.1 WRF model

The Weather Research and Forecasting (WRF) model (Skammarock et al, 2008) is a numerical weather prediction (NWP) system designed for both research and operational applications. It is suitable for use in a broad range of applications over scales ranging from meters to thousands of kilometers including idealized simulations (e.g. convection, baroclinic waves,Large Eddy Simulations), parameterization research, data assimilation research, real-time NWP and coupled-model applications.

Within the last years WRF has been extended to enable data assimilation studies. Data assimilation is the technique by which observations are combined with a NWP product (the first guess or background forecasts) and their respective error statistics to provide an improved estimate (the analysis) of the atmospheric state. Two approaches are implemented in WRFvar (WRF variational) (Barker et al. 2004) and are used in this study: Four-dimensional (FDDA) and 3dVar data assimilation.

## 2.2 Four-dimensional data assimilation (FDDA)

Four-dimensional data assimilation (FDDA), also known as nudging, is a method of keeping simulations close to analyses and/or observations over the course of an integration. The method provides a four-dimensional analysis that is somewhat balanced dynamically, and in terms of continuity, while allowing for complex local topographical or convective variations.
The method is implemented through an extra tendency term in the nudged variable’s equations (Stauffer et. al.1990, Stauffer et. al.1994). For example,

$$\frac{\partial \theta}{\partial t} = F(\theta) + G_\theta W_\theta (\tilde{\theta}_0 - \theta)$$

Where $F(\theta)$ represents the normal tendency terms due to physics, advection, etc., $G_\theta$ is a time-scale controlling the nudging strength and $W_\theta$ is an additional weight in time or space to limit the nudging, which is a value that can be set by the user. $\hat{\theta}_0$ is the time- and space-interpolated analysis field value towards which the nudging relaxes the solution. Figure 1 shows the flowchart for the WRFvar modelling system version 3 when nudging to observations. Firstly, the initialized data (the first-guess fields) from a NWP model is used as input to the WRF Pre-Processing unit (WPS). Analyses or forecast runs can be used as initial data. The WPS interpolates data horizontally to the grid-points of the model domain. The output from WPS is called met_em*. Met_em* files and observational data are used in OBSGRID to obtain grid fields for surface FDDA (wrfsfdda), observation nudging (OBS_DOMAIN) and analysis fields at surface and pressure levels (metoa_em*). Those metoa_em* files are used to generate initial and boundary conditions for WRF and the fields for upper-air FDDA.

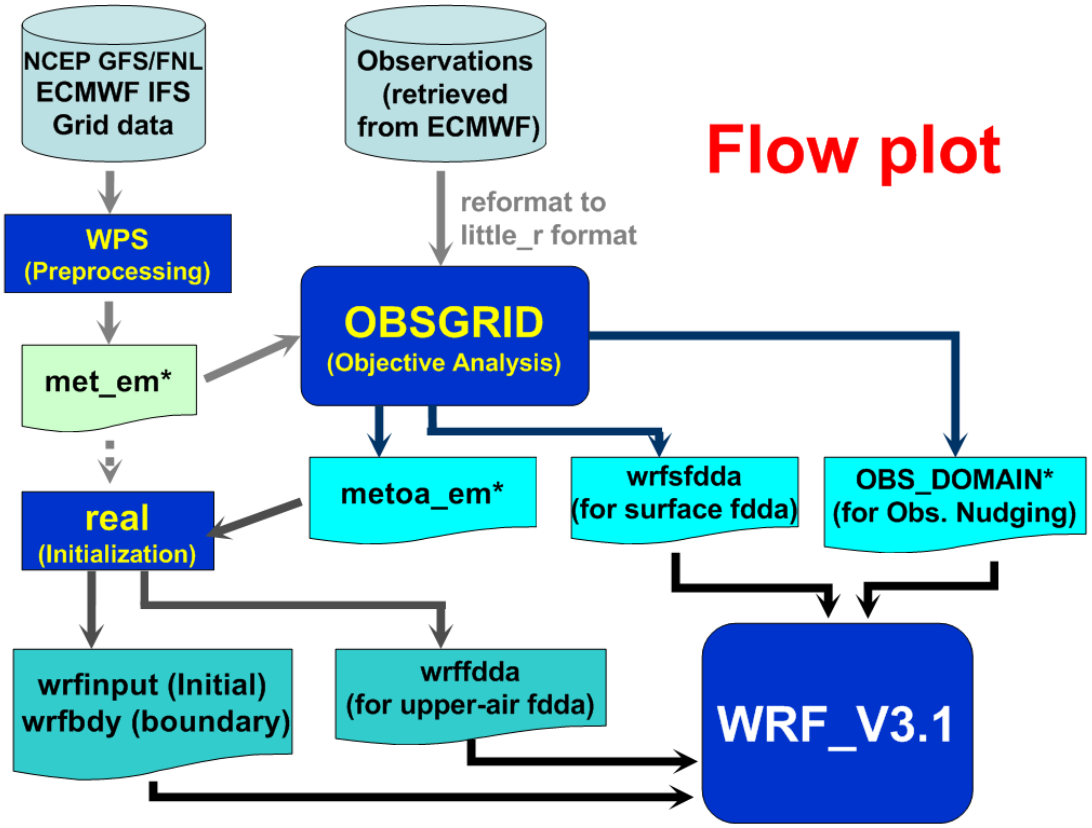


**Figure 1: Flowchart for WRFvar with four-dimensional data assimilation FDDA and objective analysis (redrawn from [WRF3]).**

## 2.3 3dVar data assimilation in the WRF-Var system

Three-dimensional variational data assimilation (3dVar) achieves the integration of observations into first-guess fields through the iterative minimization of a prescribed cost function. Differences between the analysis and observations/first guess are penalized (damped) according to their perceived error.

The basic goal of variational data assimilation is to produce an optimal estimate of the true atmospheric state at analysis time through iterative solution of a prescribed cost function (Ide et al. 1997, Barker et al. 2004):

$$J(x) = J^b + J^o$$

$$= \frac{1}{2}(x - x^b)^T B^{-1}(x - x^b) + \frac{1}{2}(y - y^o)^T (E + F)^{-1}(y - y^o) \quad \text{(Eq 1)}$$

The variational problem can be summarized as the iterative minimization of (Eq 1) to find the analysis state x that minimizes J(x). In (Eq 1), the analysis $x=x^a$ represents the "a posteriori" maximum likelihood (minimum variance) estimate of the true state of the atmosphere given two sources of data: the background (previous forecast) $x^b$ and observations $y^o$. The analysis fit to this data is weighted by estimates of their errors: B, E and F are the background, observation (instrumental) and representativeness error covariance matrices, respectively. Representativeness error is an estimate of inaccuracies introduced in the observation operator H used to transform the grid point analysis x to observation space y=H(x). This error will be resolution dependent and may also include a contribution from approximations in H. The three-dimensional variational data assimilation algorithm adopted in WRF-Var is a model-space, incremental formulation of the variational problem. In this approach, observations, previous forecasts, their errors, and the atmospheric model itself are combined to produce analysis increments $x^{a'}$ which are added to the first guess $x^b$ to provide an updated analysis. The 3dVar assimilation system in WRF is shown in Figure 2.

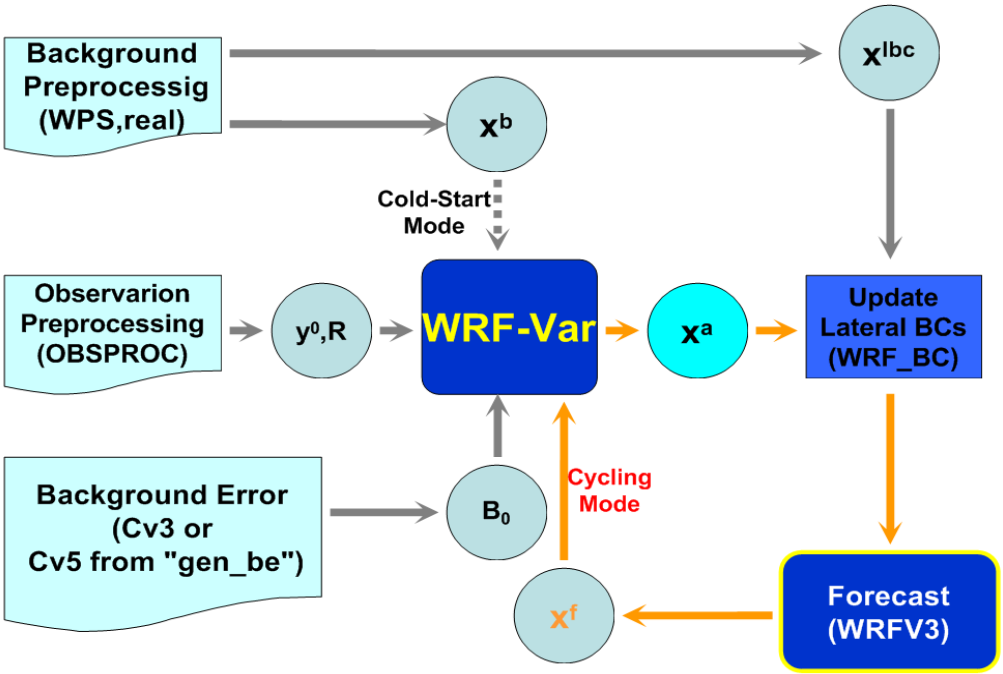


**Figure 2: Sketch showing the relationship between datasets (circles), and algorithms (rectangles) of the WRFVar system (redrawn from [WRF3]).**

# 3. Assimilation of nacelle wind speeds to improve wind power forecasts at Horns Rev

## 3.1 Introduction

With an increasing number of wind farm deployments, mostly offshore especially in Europe (Denmark, Great Britain, Germany), a new source of data is becoming available: wind speeds measured on the nacelle of a wind turbine, referred to hereinafter as nacelle winds, and the yaw angle, the turbine's angle of rotation into the wind. These wind farm observations, which up to now are primarily used by wind farm operators for control purposes, constitute a novel and unique set of measurements in the planetary boundary layer (PBL). Not many contributions can be found in the literature about the use of nacelle winds in mesoscale forecasting, none about yaw angles, to the best of our knowledge. Cutler et al. used nacelle wind speeds for power curve modelling and suggest the use of nacelle winds averaged over a wind farm in wind power forecasting.

Today many different kinds of observations are used in operational numerical weather prediction (NWP) models with the aim of more accurate forecasts by improving the analysis and subsequent forecast through data assimilation. In this study we will explore the potential benefits of wind farm observations in addition to the upper air data sets widely used in data assimilation; the area of study is the Danish offshore wind farm Horns Rev I. Since the measurements on the individual wind turbines are not independent from each other, and dealing with each turbine's measurements separately makes the data handling challenging, thinning the data is desirable. This study focuses thus on exploring different thinning strategies and their impact on analyses and shortest-term predictions, with the aim to provide the wind energy community and industry with guidelines on how to use wind farm observations for wind energy predictions.

Assimilating wind speeds measured on the nacelle of a wind turbine and the yaw angle, which serves as a proxy for wind direction, into mesoscale models is a novel approach. While data assimilation experiments have been done with various other measurements to improve the forecasts for wind farms ([Liu et al, 2011], [Delle Monache et al, 2010], [Zupanski et al, 2010]), only few conference contributions exist about the assimilation of tower measurements in the vicinity of onshore wind farms and nacelle winds using NCAR's Real-Time Four Dimensional Data Assimilation (RT–FDDA) system ([Cheng et al, 2011], [Liu et al, 2010]). To the best of our knowledge, yaw angle observations have not been used for data assimilation purposes to this date.

## 3.2 Wind farm observations

### 3.2.1 Wind farm

The wind farm Horns Rev I is located off the west coast of Denmark in the North Sea (Figure 3). It includes 80 turbines distributed over an area of 19.7 km2 in 10 rows with 8 turbines each. The distance between the turbines and from the coast is 560 m and 13.8 km, respectively. The hub height of the turbines is 70 m above MSL. Halfway between the coast and the wind farm (i.e., 6 km to the east of the farm) there is a measurement tower (referred to as M7). This tower is downstream of the wind farm during westerly winds. Another tower is located 2 km to the northwest of the farm (referred to as M2), and downstream of the wind farm for southeasterly winds. Nacelle winds and tower data are available as 10 min averages. Data used from M7 are wind speeds at 70 m and wind directions at 68 m; from M2 wind speeds at 62 m and wind directions at 43 m. We use wind direction from M2 in one experiment as a comparison to using yaw angles (section 3.5). Wind anemometers are Risø cup anemometers [Pedersen T., 2004]. To calculate pressure at 70 m with the hydrostatic assumption, which is required for the assimilation, pressure measurements at 55 m and temperature measurements at 13 and 55 m were used. Measurement masts nearby a wind farm are primarily set up to evaluate the wind potential at a site before the wind farm is built. Reliability of these data can therefore degrade if they are not well maintained after the wind farm is installed.

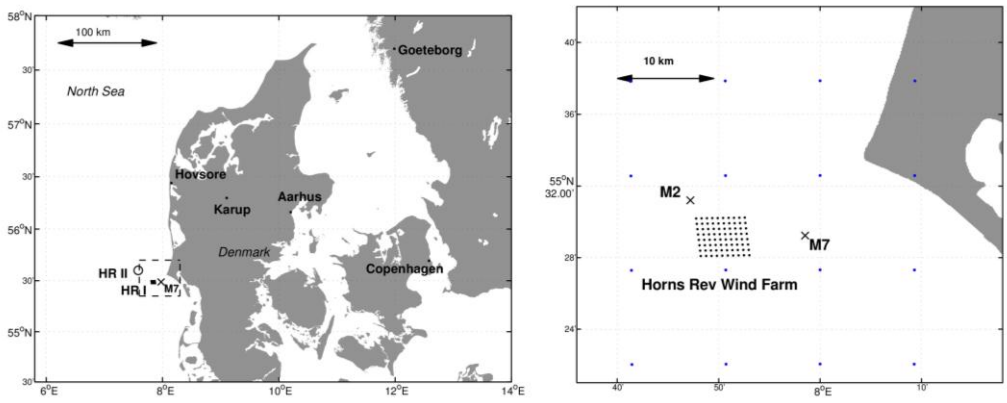


**Figure 3: Map of Denmark (left); The filled square denotes the location of the wind farm Horns Rev I, the cross the location of the measurement mast M7, and the circle the wind farm Horns Rev II. The dashed square indicates the area of the map to the right, where the dots represent the model mass grid points of domain 2, and the two crosses the measurement masts M2 and M7, respectively.**

### 3.2.2 Wind speed

Each wind turbine of the Horns Rev I wind farm is equipped with ultrasonic anemometers that are located at the back off the 10.4 m long nacelle behind the rotor. These wind measurements are typically used by wind farm operators for the turbine control, to determine cut-in/cut-off wind speeds. Since the anemometers are situated behind the rotor, they do not measure the free wind conditions from that region but are disturbed by the turbine-induced turbulence. This
disturbance depends on the design/shape of the wind turbine and nacelle, the pitch/stall situation, whether the turbine is operating or not, the yawing errors (i.e., the difference of wind direction between the free wind and the alignment of the turbine), the height of the anemometer and its position on the nacelle [Zahle and Soerensen, 2011], [Smaili and Masson, 2004]. For data assimilation the information from the free wind conditions at a site is required, and deviations from representative wind speeds need to be accounted for. Since the wind disturbances are very complex, a general valid correction of these data is an ongoing field of research.
Nacelle anemometers are generally calibrated with a nacelle transfer function which describes the undisturbed wind field [Frandsen et al, 2009]. This function is determined empirically by comparing wind measurements from a tower situated approximately 250 m upwind to nacelle anemometers, and can be derived for both wind speed and direction; some of the limitations of this approach are the non-consideration of turbulence effects, vertical inflow or upflow conditions. Furthermore, these functions are based on a reference turbine and therefore do not account for local conditions or park effects ([Zahle and Soerensen, 2011], [Antoniou and Pedersen, 1997]). Most turbines are equipped with two anemometers, on the right and left side of the nacelle. When data transfer problems or data overload occur, the received signal can switch from one anemometer to the other one. The observations reported by the two anemometers can be slightly different, adding to the complexity of the issue [Rolf-Erik Keck, personal communication, December 2010]. In addition to the disturbance included by the turbine's rotor, nacelle winds are affected by wakes generated by upwind turbines. Energy losses due to wakes can be in the order of 5-15 % of a whole wind farm ([Barthelmie et al, 2010], [Barthelmie and Jensen, 2010]) and the wind speed reduction can be up to 20 % for certain turbines depending on their position in the wind farm, which can result in a wind loss of a few ms−1. However, wake modeling of large wind farms is still subject to an unacceptably high degree of uncertainty [Barthelmie et al, 2010]. Wake effects depend on atmospheric stability and wind speed ([Christiansen and Hasager, 2005], [Barthelmie et al, 2010]). Figure 4 shows time series of nacelle winds for the first five upwind turbine rows and the 70 m measurements of mast M7 on May 29 2005. Their behaviour is representative for all the test cases in this study (section 3.4.2). The wind hits the farm from the west; the wind speeds from the mast were lower than the ones from the turbines in row 1, but less difference between the mast measurements and the turbine measurements can be seen for the downstream turbine rows, indicating wake effect for these rows. This further indicates a slight wake effect on mast M7 since the measurements correspond best to the wake contaminated nacelle winds from row 5. Alternatively,

since the wind farm is close to the mainland of Denmark, land blocking can contribute to this effect. The 70 m measurements from M7 downwind show a lag around 14:30 UTC, which can be explained by the distance of 6 km between the farm and the mast. The nacelle winds from each row were within an interval of approximately 1 ms−1.

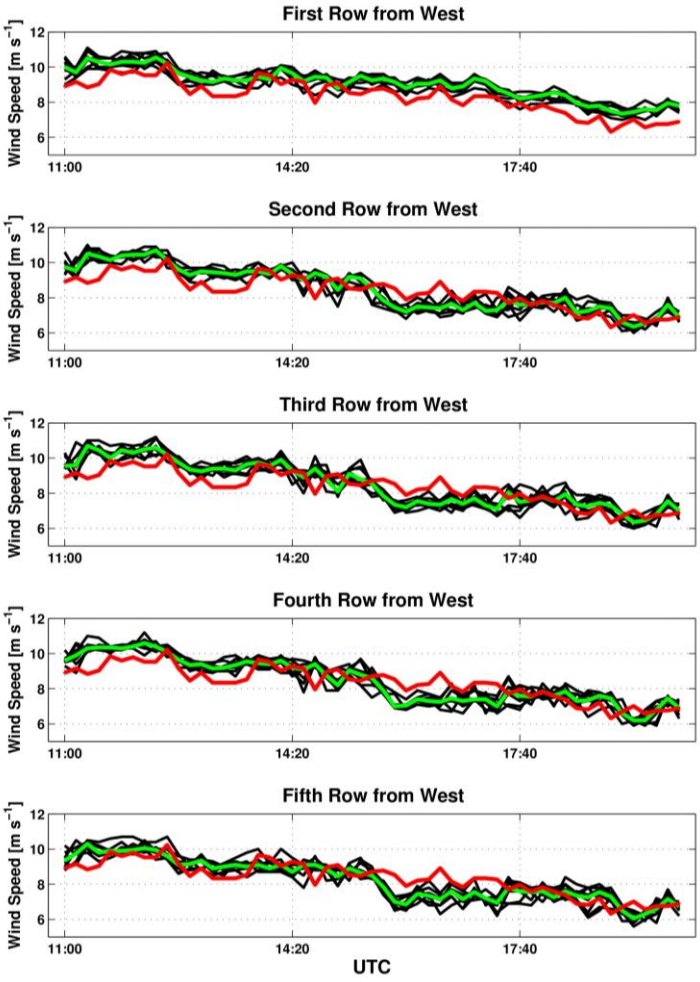


**Figure 4: Time series of nacelle winds (individual turbines in black, median in green) and wind speed measurements from measurement mast M7 at 70 m (red) for each turbine from the westernmost row of the wind farm (upper panel), the second row from the west (second panel), the third row (third panel), the fourth row (fourth panel) and the fifth row from the west (fifth panel). The wind on this day (29 May 2005) came directly from the west.**

### 3.2.3 Wind direction

Modern turbines turn into the wind following the wind direction measurements provided by the nacelle anemometers. This rotation, referred to as the yaw angle, is available as a proxy for wind direction. Depending on the turbine type, turbines yaw quickly: common MW-turbines yaw at a rate of about 0.5 ◦ sec−1. They use averaging algorithms, and typically yaw when they have reached an averaged yaw-error value of about +/- 5°. Then they yaw until they have reached the center value again. As with nacelle winds, yaw angle estimates are affected by errors. First, the measured wind direction to determine the yaw error is error prone [Zahle and Soerensen, 2011]. Yaw errors appear to be on the average up to 10° [Pedersen et al, 2010] and are a result of the difference between the free wind direction and the measured direction of the disturbed wind behind the rotor. Second, below the common cut-in wind speed of 4 ms−1 and above cut-off wind speeds of 25 ms−1 the turbine is not operating and thus not yawing. Upon restart, the turbine starts operating from a random position, and it takes time for the sensor to be correctly oriented again, resulting in raw yaw data that may be

misleading. However, since the orientation of the sensor should last less than a minute, only the time when the turbine is not yawing needs to be flagged by a quality control procedure. An additional complication is the fact that the turbine cables have to be disentangled after a number of nacelle rotations, and the yaw has to be re-oriented again. Third, each wind turbine has a different offset in yaw angle. A research project [Kurt S. Hansen, personal communication, Dec. 2010] led to the correction of the yaw angle offset for Horns Rev's turbine 7, and this is the only turbine's yaw data used in our experiments as proxy for wind direction. Indeed, comparisons of yaw angles with wind direction measurements from a downwind mast show quite good agreement during our experiments. The agreement of mast data and yaw angles shown in Figure 5 is representative for all the test cases in this study. The time series of the yaw angle are smoother than the ones from M7, which might be an advantage in the assimilation process, because they might fit better to the hourly model values and thus not be eliminated by the data misfit or quality control procedures. The lag shown with respect to M7 is probably due to the distance of 6 km. Yaw angle data were available as 10 min averages.

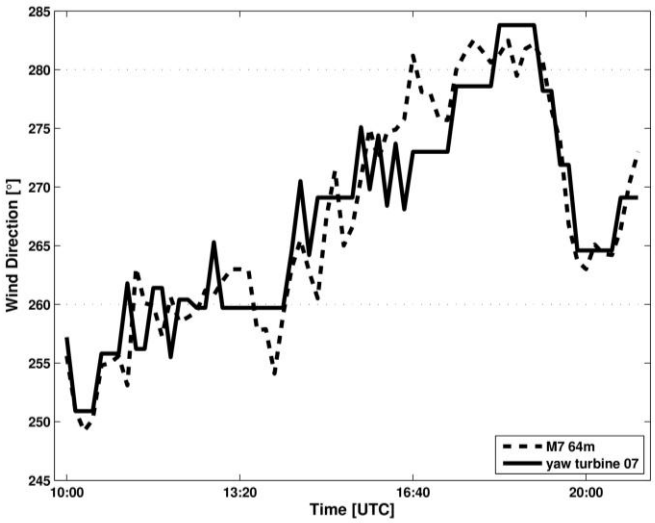


**Figure 5: Yaw angle from turbine 07 and wind direction from measurement mast M7 collected on 29 May 2005.**

For data assimilation applications, wind direction values can also be taken from the model or from mast measurements. However, mast data in the vicinity of wind farms are less frequently available than yaw angles, and therefore the latter have been used in our experiments. We did not use the available wind direction measurement from the sonic anemometer on the nacelle for the following reason: since the sensor on the turbine turns with the turbine, the measured wind direction is the difference between the true wind direction and the yaw, i.e., the position of the nacelle in the wind. During easterly winds for example, if the turbine is aligned correctly, the indicated wind direction will be the same as during a correct alignment during westerly winds.

## 3.3 Data assimilation system

We used the Four Dimensional Data Assimilation (FDDA) system of the WRFvar model (see section 2) in version V3.2.1 [Skammarock et al, 2008], which is based on Newtonian relaxation (i.e., nudging). As described in section 2.2 this data assimilation method relaxes the model state toward the observed state by adding tendency terms based on the difference between the two states to one or more of the prognostic equations [Stauffer and Seaman, 1994]. We used the approach of nudging directly toward individual observations, which are distributed non-uniformly in space and time (obs nudging). This approach uses only those observations that fall within a predetermined time window centered about the current model time step. In our set up, the half time window for domain 1 was 0.8 hours, for domain 2 it was 0.6 hours. The differences between the model and the observed state are computed at the observation locations. These corrections are then analysed back to the grid within a region of influence surrounding the observations. The assimilated data sets included wind farm data and upper air observations of the Meteorological Assimilation Data Ingest System (MADIS). The latter comprised

data from the Aircraft Communication Addressing and Reporting System (ACARS), and observations from radiosondes; a snapshot of their typical distribution is shown in Figure 6. Observations were assimilated hourly during a pre-forecast period of 24 hours to provide initial conditions for each of the test cases described in section 3.4.2, and for the time of the test cases thereafter to produce initial conditions. The control run where no data assimilation was performed (CTL) was spun up without nudging. After the spin up period, free 24-hour forecasts were initialized from the resulting analyses every hour. For the selected cases this resulted in 44 24-hour forecasts.

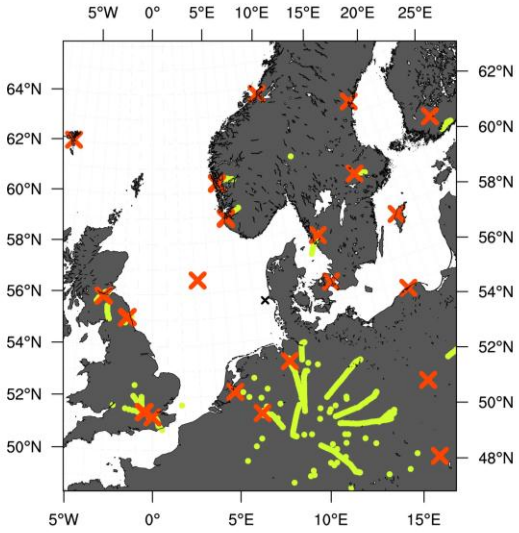


**Figure 6: A snapshot of the distribution of observation locations on 20 July 2005 at 12 UTC. Radiosonde observations (red cross) and ACARS (green dots) were used in the assimilation. The black cross denotes the location of Horns Rev.**

The model setup for the experiments consisted of an outer and a nested domain with horizontal grid increments of 30 and 10 km, respectively (Figure 7). The model was initialized and forced at the boundaries by 1°x1° U.S. National Center for Environmental Prediction (NCEP) Global Forecast System 6-hour forecasts. The sea surface temperature fields were also obtained from NCEP analysis at a horizontal resolution of 0.5°x0.5°. We used 1-way nesting and 37 vertical levels, with 7 levels within the lowest 500 m. The lowest levels important for wind energy applications were at approximately 16, 59, 117, and 183 m AGL. The model physics options include: Yonsei University (YSU) boundary layer scheme, Lin et al. microphysics scheme, MM5 similarity surface layer, Noah land surface model, and the Kain-Fritsch cumulus parameterization. The model dynamics options include: 2nd-order diffusion with a horizontal Smagorinsky first order closure, 6th-order numerical diffusion with prohibit up-gradient diffusion for the inner domain, and positive-definite advection of moisture and scalars (for more detail see [Skammarock et al, 2008]). These model configurations were chosen based on experiences from previous modelling systems and sensitivity experiments at DTU Wind Energy.

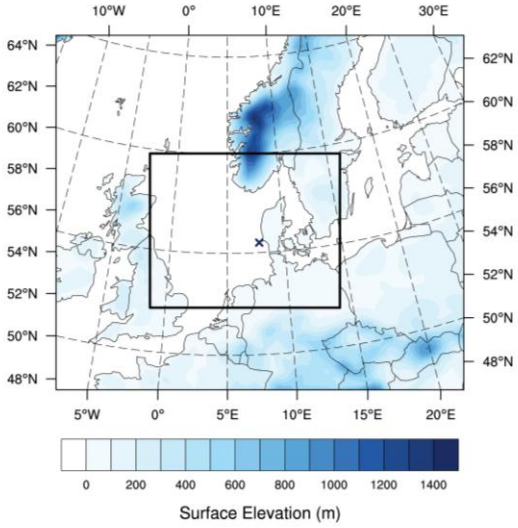


**Figure 7: Domain configuration and terrain elevation of WRF model setup. The squares indicate the boundaries of nested domain and the cross the location of the wind farm Horns Rev I.**

## 3.4 Methods

### 3.4.1 Thinning strategies

Wind farm data are spatially dense and, compared to a mesoscale model grid with grid spacings between 2 and 30 km, many observations are in the subgrid space (Figure 3, right panel). Thus, the measurements do not provide independent information and dealing with each turbine's measurements separately makes data handling challenging and increases the computational costs [Lazarus et al, 2010]. Additionally, in data assimilation systems like the Ensemble Kalman Filter or variational methods, datasets with a high spatial density violate the assumption of spatially independent observation errors (e.g., [Daley, 1991] or [Ochotta et al, 2005]). Therefore, a procedure is needed to reduce the amount of data and produce a representative data set.

Thinning is also a way to deal with the inherent issues associated with wind farm data (section 2.2 and 2.3). The thinning strategies consist of different grouping strategies of nacelle winds. In this study, we calculated median nacelle winds of the first upwind turbine row, the second upwind row, the third upwind row, the fourth upwind row, the fifth upwind row, all the turbines, the upwind half of the wind farm and the first two upwind turbine rows combined. We chose the median over the mean to avoid the negative effect of outliers. Nacelle winds were quality controlled to remove erroneous data in the data set, but not ”cleaned” to account for their inherent issues, e.g., for wake or wind farm effects. For the assimilation experiments, wind directions come from the yaw angle of turbine 7 (situated in the first upwind row) and additionally from measurement mast M2 at 60 m for the group with medians of the first two upwind rows. The metrics used to evaluate the best thinning strategies were the root-mean-squared error (RMSE), bias, centered root-mean-squared error (CRMSE) and rank correlation. The RMSE is the metric that is best known and commonly used. It can be split into the bias and centered root-mean-squared-error (CRMSE) [Taylor, 2001]. The bias is a measure of the systematic component of forecast error, which may come from the model misrepresentation of topography/coastlines, offset parameter values, biased initial conditions, etc. [Delle Monache et al, 2011]. The CRMSE is considered the random component of the error. It gives an indication of the intrinsic predictive skill of the forecast that can be limited by the coarse or non-existent representation of specific physical processes, which is often harder to get rid of in a forecasting system than the systematic bias. . The rank correlation is a nonparametric (i.e., distribution free) statistic that reflects the strength of the monotone relationships between two variables [Wilks, 2006]. As such it allows for a nonlinear relationship between the predictions and observations, which is appropriate when the quantity of interest, wind speed in this study, exhibits a non-Gaussian distribution and quantifies pattern similarity [Delle Monache et al, 2011]. High correlation values indicate better pattern similarity. This is especially important in wind energy forecasting where a correct prediction of patterns, e.g., the onset of a ramp event (large and rapid changes in wind speed) is extremely valuable.

### 3.4.2 Test cases

Suitable test cases were selected to study the assimilation impact of wind farm data following the different thinning strategies. We are particularly interested in the impact of the assimilation at the location of the observations, i.e., the wind farm, as well as at downwind locations. The latter is important for the wind energy industry to understand if data collected at a wind farm could be useful for shortest-term predictions at a nearby downwind farm. This is the case at Horns Rev I, which is situated downwind of the wind farm Horns Rev II during westerly winds (Figure 3). Data from the adjacent wind farm Horns Rev II were unfortunately not available at the time this research was performed.
Since M7 is situated directly east of Horns Rev I, we selected cases with westerly winds (i.e., winds between 260° and 280°). Restricting the cases to westerly winds would also allow us to define unchanging upwind rows. During westerly winds M7 could be affected by wakes of the wind farm. The selected periods were thus further restricted to periods where wind speeds at M7 were within 5 % of mast M2, the mast to the northwest of the farm and not in the wake during westerly conditions. This was to ensure impartial verification with minor wake effects at M7. Results with Risø's wake model WAsP Engineering (http://wasp.dk) confirmed minor wake effects on M7 below 1.6 $ms^{-1}$ during the test cases (not shown).

Due to these limitations only 5 cases with varying length in May, July, August and October 2005 were found with simultaneous measurements on the turbines and the measurement masts out of 10 years of recorded data. Given that we analysed 24-hour forecasts the restrictions will be valid only during the time of the analyses and at least for the first three forecast hours. For later lead times wind conditions may change.
Denmark is situated around 56 degrees north with prevailing westerly winds. The selected test cases with winds from the west are thus representative. During the experiments the conditions at the wind farm Horns Rev were associated with a low pressure system over northern Europe/Scandinavia and/or a cold front passage (Table 1, Figure 8).

**Table 1: Date and weather conditions for the selected test cases. The dates denote the analyses that were used to initialize the forecasts.**

| Test case | Weather conditions at Horns Rev |
|---|---|
| 29 May 11 UTC - 29 May 17 UTC | A low pressure system over the British Isles and southern Scandinavia led to southern winds in 500 hPa and westerly winds near the surface. During the course of the day high pressure took over from the south, leaving Horns Rev all day in a westerly flow |
| 19 July 13 UTC - 20 July 05 UTC | Low pressure dominated Scandinavia and the British Isles, with its core moving from the north of the British Isles westward, leaving Denmark to the south of it in a westerly flow. A trough axis passed over western Denmark before the case. Precipitation was associated during this case |
| 26 Aug. 00 UTC - 26 Aug. 04 UTC | Low pressure was dominating over Northwest Europe, leading to westerly flow with convective conditions at Horns Rev |
| 26 Aug. 13 UTC - 26 Aug. 18 UTC | Low pressure was dominating over Northwest Europe, leading to westerly flow with convective conditions and showers at Horns Rev |
| 25 Oct. 16 UTC - 26 Oct. 00 UTC | Low pressure was dominating over northern Europe, with its center located over southern Norway at 18 UTC. A cold front was associated with the low, which had passed Horns Rev around 12 UTC on October 25th. Denmark was in a westerly flow and precipitation was associated with this case |

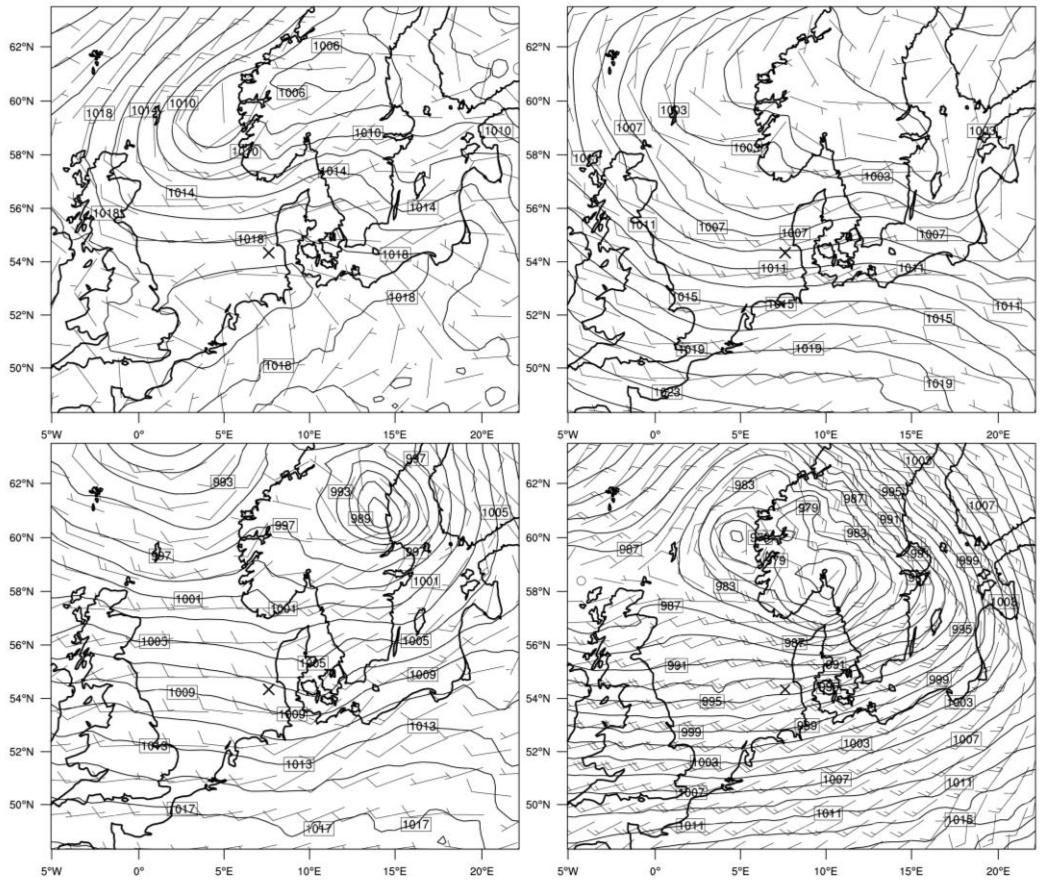

**Figure 8: Maps of sea level pressure during the test cases: 29 May 2005 at 15 UTC (upper left), 20 July 2005 00 UTC (upper right), 26 Aug. 2005 at 12 UTC (lower left) and 25 Oct. 2005 at 18 UTC (lower right). Only one map is shown for the August cases since they are on the same day. Overlaid are wind barbs on the second model level (~59 m); half ticks represent 5 ms$^{-1}$, full ticks 10 ms$^{-1}$. The cross denotes the location of Horns Rev I.**

## 3.5 Results

### 3.5.1 Impact of thinning strategies

As described in section 3.4.1, thinning techniques are necessary for wind farm data to be assimilated into a NWP model. Our study focuses on quantifying the data assimilation impact on wind speed forecasts downwind at M7 and at the wind farm itself. We thus calculated error metrics (bias, RMSE, and rank correlation) for different groups of turbines using the wind measurements from M7 as a reference. This serves as an estimation of which group (i.e., thinning strategy) would have the potential to be successful in the assimilation experiments. The groups were: median winds of the first upwind row (Row 1), the second upwind row (Row 2), the third upwind row (Row 3), the fourth upwind row (Row 4), the fifth upwind row (Row 5), all the turbines (all), the upwind half of the wind farm (half) and the first two upwind turbine rows combined (Rows1&2). These groups were ranked by bias, RMSE and rank correlation, and these rankings were summed to select a subset presenting the best thinning strategies. The turbine aggregations that exhibited the lowest RMSE, rank correlation, and bias combined were used in the assimilation experiments. These were the median of the first two upwind turbine rows together, followed by the median of the first row and the median of all the turbines (Table 2).

**Table 2: Root mean square error, Pearson correlation and bias of nacelle wind aggregations with regard to wind speeds at M7 at 60 m, and their ranking for the median winds of the first, second, third, fourth, fifth upwind turbine row, all the turbines, the upwind half wind farm, and rows one and two together for all the test cases combined. For error metrics of all the test cases separately see Table 4.**

| Aggregation | RMSE | Rank RMSE | CORR | Rank CORR | BIAS | Rank BIAS | Total Ranking |
|---|---|---|---|---|---|---|---|
| Row 1 | 1.106 | 2 | 0.943 | 1 | 0.323 | 2 | 5 |
| Row 2 | 1.226 | 5 | 0.925 | 6 | -0.353 | 4 | 15 |
| Row 3 | 1.266 | 7 | 0.922 | 8 | -0.414 | 6 | 21 |
| Row 4 | 1.253 | 6 | 0.923 | 7 | -0.407 | 5 | 18 |
| Row 5 | 1.284 | 8 | 0.929 | 4 | -0.585 | 8 | 20 |
| all | 1.221 | 4 | 0.938 | 3 | -0.571 | 7 | 14 |
| half | 1.204 | 3 | 0.928 | 5 | -0.342 | 3 | 11 |
| Rows 1&2 | 1.065 | 1 | 0.941 | 2 | 0.019 | 1 | 4 |

The medians of wind speed of the first two upwind rows are usually higher than the ones for the other groups due to wake effects on the rows further downwind. One exemplary short time series is shown in Figure 9. The median of all the turbines is lower, because it includes the lower wind speeds from the wake affected turbines downwind. Generally, the difference between the groups is within 1–2 ms−1. The bias of all the groups is mostly negative, that means that the wind speeds of M7 are higher than the ones from the groups; the correlation is highest for turbine 1 most of the time - which indicates that the wake effect on M7 was very small. Wake meandering will have an impact on these results as well, but we have not attempted to quantify it.

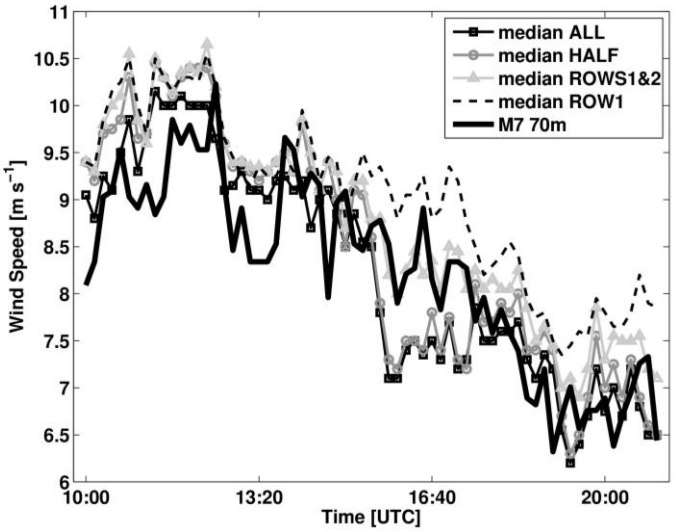


**Figure 9: Time series of median wind speeds of the groups ALL, HALF, ROW1 and ROWS1&2 (Table III) as well as of the 70 m measurements at M7 for the case from 29 May 2005. The median of ROW1 is higher than the others, which is representative for all the cases.**

### 3.5.2 Impact of the assimilation

Nacelle winds differ from one wind turbine to another because of wake effects as well as operational constraints. Therefore, the medians of different thinning techniques vary (Figure 9). In this section we analyse the impact of assimilating wind farm data and of the selected thinning techniques. We assimilated the median of the whole wind farm (ALL), the median of the upwind half wind farm (HALF), the median of the first upwind turbine row (ROW1) and the median of the first two upwind turbine rows.

The wind direction data source for all the experiments was the yaw angle from turbine 7; for Rows1&2 both the yaw angle (ROWS1&2YAW) and the direction measurements at M2 (ROWS1&2M2) were used to evaluate the sensitivity of different wind direction data sources. Note, that upper air MADIS data were assimilated additionally to the wind farm observations. The experiments are summarized in Table 3.

**Table 3: Experiments including the thinning strategy adopted and the wind direction data source. Note that all the experiments assimilated upper air MADIS observations additionally to wind farm data.**

| Experiment | Thinning strategy | Wind direction |
|---|---|---|
| ALL | Median of whole wind farm | yaw angle |
| HALF | Median of upwind half wind farm | yaw angle |
| ROW1 | Median of upwind row | yaw angle |
| ROWS1&2M2 | Median of first two upwind rows | 43 m from M2 |
| ROWS1&2YAW | Median of first two upwind rows | yaw angle |
| MADIS | only upper air MADIS data assimilated | N.A. |
| CTL | no data assimilation performed | N.A. |

The results show a positive impact of the assimilation of both MADIS and wind farm data beyond 24 hours (Figure 10). The impact of the wind farm data assimilation is evident in the first 2 hours for the bias (Figure 10a, experiment ALL vs. MADIS). The difference between the thinning techniques is most pronounced for the analysis. Beyond a 2 hour time scale, the assimilation impact of wind farm data together with MADIS data is similar to the assimilation with only MADIS data, indicating the benefit of upper air MADIS data in the assimilation. The average distribution of these data covers most of the model domain and includes upstream data (Figure 7), which explains the long assimilation impact beyond 24 hours. Since the location of M7 and Horns Rev is only one grid point apart, with a radius of influence of 90 km this results in minor differences between the two locations. Detailed results will be explained in this section.

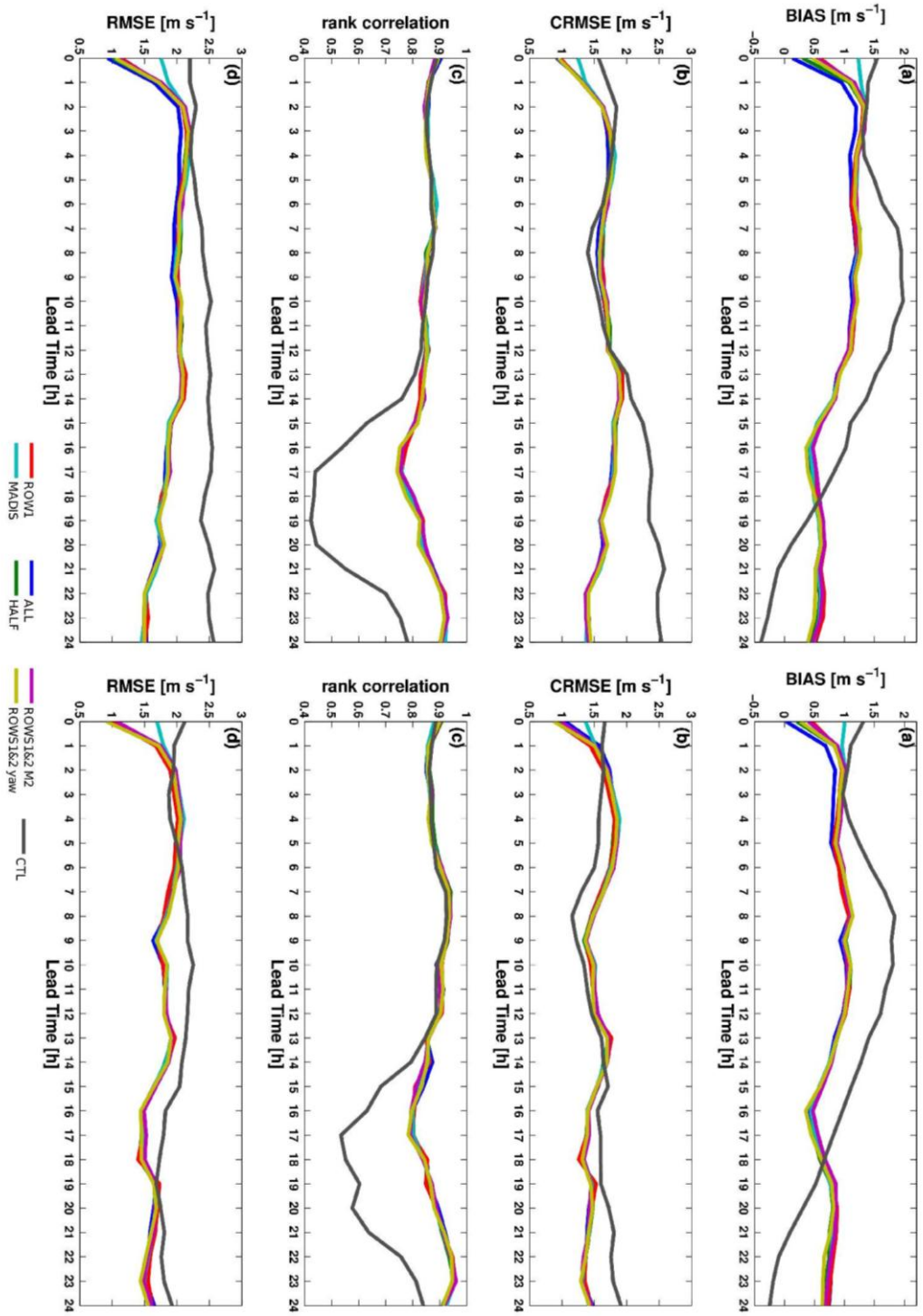


Figure 10: Bias (a), CRMSE (b), Rank correlation (c) and RMSE (d) of wind speed for the experiments described in Table 3, and for 0–24 h lead times at M7 (left) and Horns Rev (right). The reference for the metrics (i.e. the observations) for Horns Rev is the median wind speed from ROW1.

### 3.5.2.1 Assimilation impact depending on lead times up to 24 h

The bias at M7 (Figure 10a, left) was reduced by all the assimilation experiments compared to the CTL up to a lead time of 18 hours. Especially up to lead time 2, the assimilation of wind farm data reduced the bias also compared to assimilating only MADIS data. . The assimilation impact on the bias beyond the advection timescale is suspected to be the result of the altered atmospheric state due to the data

assimilation procedure. While the bias of the experiments decreases slightly from 1.3 ms−1 to 1 ms−1 for lead time 1 – 12, the bias of the CTL is slightly reduced up to lead time 4 with a rapid increase around lead times 6 – 12. The low but increasing bias for the first two lead times points at advection of the data assimilation impact downstream to M7. Similar conditions apply for Horns Rev (Figure 10a, right).
The CRMSE (Figure 10b, left), is reduced by the assimilation experiments compared to the CTL for the first 4 lead times and from lead time 12 onwards. However, in between these lead times the CTL experiment has similar error scores. This and the increase of CRMSE after lead time 1 at Horns Rev compared to the CTL suggests the introduction of numerical noise through the assimilation (Figure 10, right). The RMSE (Figure 10d, left) shows the added contributions of CRMSE and bias. The RMSE at M7 is reduced by the assimilation for all simulated lead times and even beyond that. The assimilation of wind farm data outperformed the MADIS experiment up to lead time 2. Experiment ALL shows the best results, and its impact is visible far beyond the advection time scale. At Horns Rev, the contribution of CRMSE to the RMSE led to improvements up to lead time 1 and from 6 – 24. Here, the increase in CRMSE after lead time 2 led to a better performance of the CTL for lead times 2 – 5. The rank correlation (Figure 10c, left) is similar for all the experiments and is nearly constant for the experiments where data assimilation was performed, whereas the correlation of the CTL drops considerably after lead time 12. Note, that Figure 10 shows average error metrics over all the cases. The error metrics for all the cases separately show different features (not shown). We attempt to analyse the impact of the data assimilation further in sections 3.5.2.3 and 3.5.2.4.

#### 3.5.2.2 Difference in thinning techniques 0 – 6 hour for lead times

The distinction between the thinning techniques is most pronounced during the first 5 lead times (Figure 11, left). The experiments using the yaw angle slightly outperform the ones using the wind direction measurements from M2 to the north of the farm. This is an advantage, because if the yaw angle data are known to be reliable for data assimilation, there is no need to additionally set up an expensive measurement mast. Moreover, only wind farm data, which are recorded for control purposes in any case, have the potential to contribute successfully to the assimilation experiments. The verification with M7 data shows that the bias is positive. The bias was reduced compared to the CTL, but also compared to the run with only MADIS data (Figure 11a, left). Experiment ALL shows the best result. The bias of ALL increases from lead time 0 – 2, but is still the lowest during the first 6 lead times. The increase in bias up to lead time 2 for all the data assimilation experiments could be due to increased noise in the simulations. For the CTL the pattern looks different: a slight reduction in bias until lead time 3, followed by a steep increase. Experiment ALL assimilated the median of all the turbines, which is lower than the one from other group. As such it is more similar to M7. Moreover, when verifying with the wind farm itself (i.e., with the median of ROW1 for all the cases), ALL shows the best results as well during the first 5 hours (Figure 10a (right)), even though ROW 1 would be expected to have an advantage as the reference. This is because the assimilation decreases the wind speeds in the model estimate. ALL is showing the lowest median wind speeds (Figure 9), and thus most successful in doing so. The CRMSE (Figure 11b (left)), was reduced by the assimilation of wind farm data up to lead time 4 compared to experiment MADIS and the CTL, which shows the ability of the assimilation to add predictive skill to the raw forecast. One could argue that the bias of 1 ms−1 can be the outcome of wake effects on M7. However, this effect does not explain the behaviour of CRMSE. The different thinning techniques show similar behaviour at the location downwind and the wind farm itself; for Horns Rev, the benefit of the assimilation does not go beyond lead time 2 for the CRMSE (Figure 10b (right)). The results for the bias and the CRMSE combined, shown as the RMSE in Figure 11d (left), clearly demonstrate that ALL outperforms the other experiments for the verification with M7. The rank correlation (Figure 11c, left) shows little variations (0.1%) between all the experiments for lead times 0 – 6.

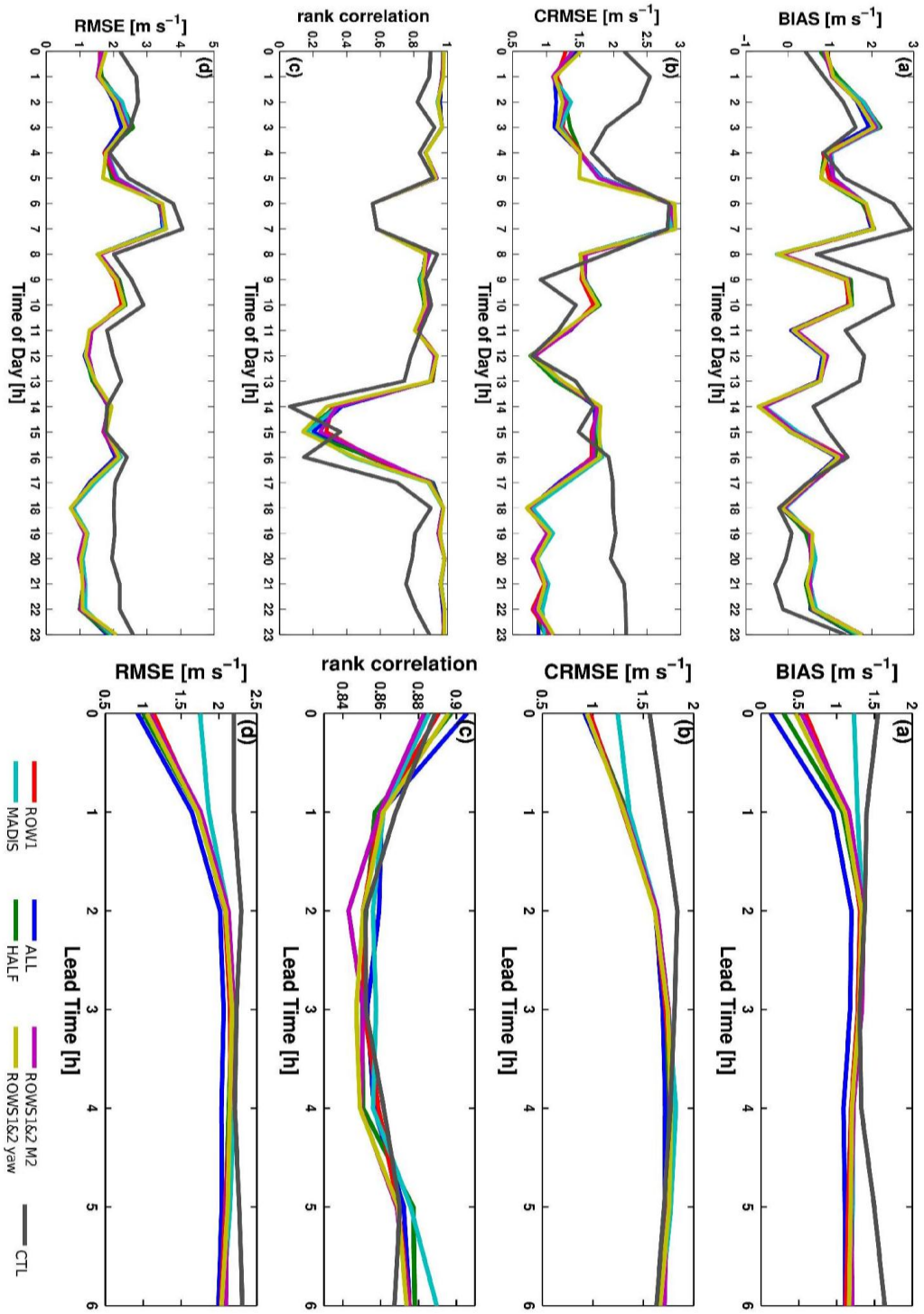


**Figure 11: Right: Same as Figure 10 (left), but for 0–6 h forecast lead times. Left: Bias (a), CRMSE (b), rank correlation (c) and RMSE (d) of wind speed for the experiments described in Table III, and for each hour of the day (valid time in UTC) at M7.**

### 3.5.2.3 Assimilation impact depending on time of day

The results in the figures discussed above show the assimilation impact on the forecast lead time, but do not give information about the dependence of the results on the valid time, i.e., time of the day. Bias, CRMSE, rank correlation and RMSE of M7 were thus averaged over their valid time in Figure 11

(right). Due to the relatively small sample size during each time of the day, the curves are uneven. However, the CTL and data assimilation experiments are distinct. The bias and CRMSE show a mirrored behaviour: whereas the systematic error was improved during the day between 5 and 16 UTC and declined during the night between 16 and 4 UTC by 0.5 ms−1, the CRMSE was improved during the night between 16 and 6 UTC by 1 ms−1. During the day the simulations with and without data assimilation perform similarly for CRMSE. The times of transition between improvement and decline of the error metrics in the afternoon coincide approximately with the transition from day time to night-time conditions in the atmosphere (convective and stable boundary layers, respectively). The rank correlation was improved during the first lead times up to 5 UTC and after 11 UTC. Both the assimilation experiments and CTL show a deep drop in correlation around 14 – 16 UTC. This indicates, that the drop in rank correlation for the CTL in Figure 10 was related to the valid time rather than on lead time and averaged out for the assimilation experiments. The behaviour in bias and CRMSE combined is reflected in Figure 11d (right), which shows an improvement of data assimilation experiments throughout the whole day, except for 3 – 4 and 14 – 15 UTC. The behaviour of all the assimilation experiments is similar.

#### 3.5.2.4 Analysis of forecast error

Figure 12 shows a break-down of the forecast error for all the simulated lead times for the CTL and experiments ALL, HALF and ROW1 to have an overview of the assimilation impact.

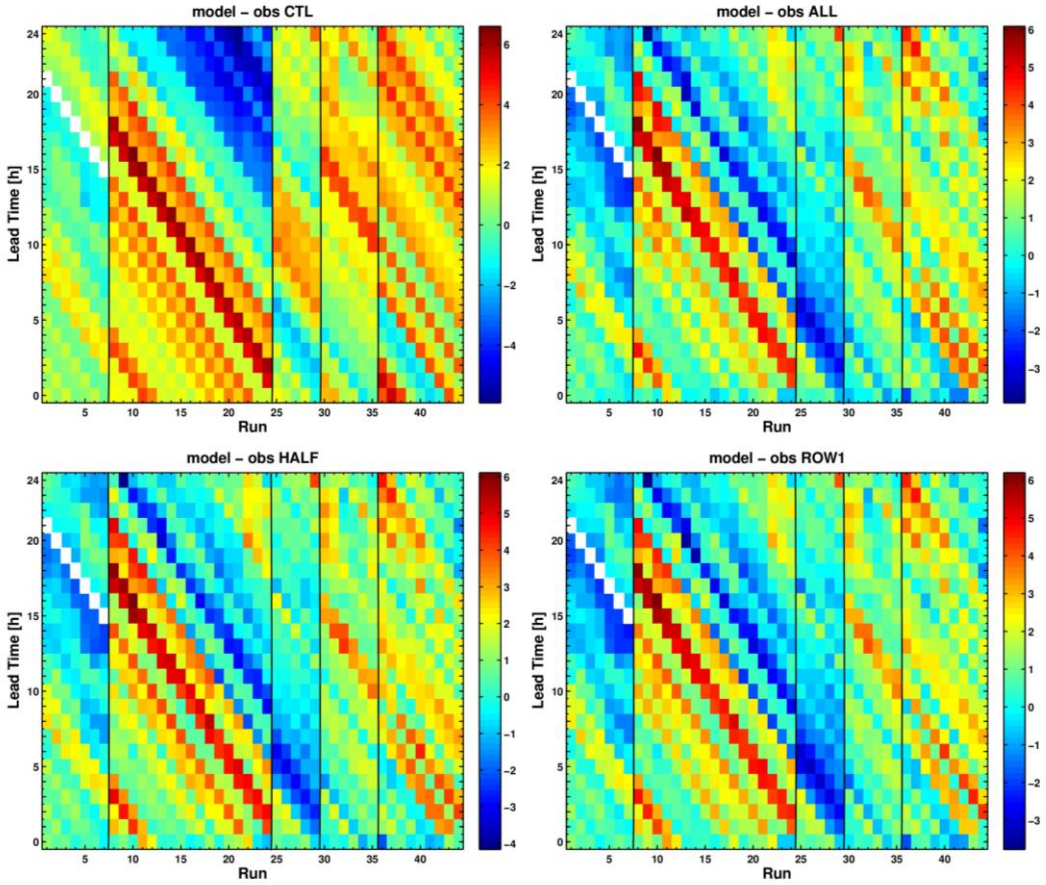


**Figure 12: Break down of the wind speed error (model minus observation) as a function of data assimilation experiment (Run; x-axis) and lead time (y-axis) for the CTL (left) and experiments ALL (upper right), HALF (lower left), ROW1 (lower right) at M7. Every coloured square represents the forecast error at a particular forecast hour. The black vertical lines separate the test cases from each other. Data void areas are left white.**

The forecast error is shown as a function of data assimilation experiment (Run, x-axis) and lead time (hours, y-axis), thus every coloured square represents the forecast error at a particular forecast hour. The black vertical lines separate the test cases from each other. All the experiments show similar results with minor differences for specific hours (not shown for ROWS1&2 and MADIS). The experiments succeeded in decreasing the forecast error in many cases, which is indicated by more blueish/greenish colours in Figure 12 (upper right and lower panels) compared to the CTL (Figure 12 upper left). This is in agreement with the results in Figure 10a (left), where the positive bias was decreased. The diagonal patterns suggest that the forecast error does not primarily depend on a specific lead time, but on a specific valid time. However, since the diagonal patterns are not consistent throughout the cases, the error depends rather on a specific weather situation at a certain time of the day. This is confirmed by Figure 13, which indicates the dependence of the error on time of the day for all the experiments. Moreover, the CTL shows a stronger and more consistent line pattern than the assimilation experiments, indicating stronger dependence on weather situation. The diagonal patterns in Figure 13 (middle panel) for the CTL for e.g., runs 9 – 18 and valid times 14 – 23 are not clearly visible in the assimilation runs (Figure 13, top panel). Diagonal signals indicate a dependence on lead time. In this specific example the analysis (lead time 0) in the CTL has a different error behaviour than the following lead times. Since that clear signal of diagonal line is only slightly visible in the assimilation runs, this indicates that in the assimilation experiments especially the error of the analysis was improved. At the same time, since the diagonal pattern in this example is not continuous, there is an impact on weather situation discernible as well. The dependence on the weather situation can further be seen in Figure 13 (lower panel), which shows the absolute differences of errors (the errors of the assimilation experiments minus the error of the CTL). While the differences between the errors of the CTL and the assimilation experiments are mostly very low (blue colour), 3 blocks of higher differences stand out: The red triangle shaped blocks during runs 15 – 24 and the squared greenish blue block during runs 25 – 29. Although the performance of the experiments compared to observations was not evaluated in this figure, it shows very well the impact of the assimilation in terms of difference to the CTL and indicates weather dependence once again. During case 2 and 3 the differences were most pronounced. During case 2 the CTL exhibited a negative bias during the night, which could be successfully declined by the assimilation. The absolute error difference during case 3 is due to a positive model bias around noon, which was reduced by the assimilation to a negative bias.

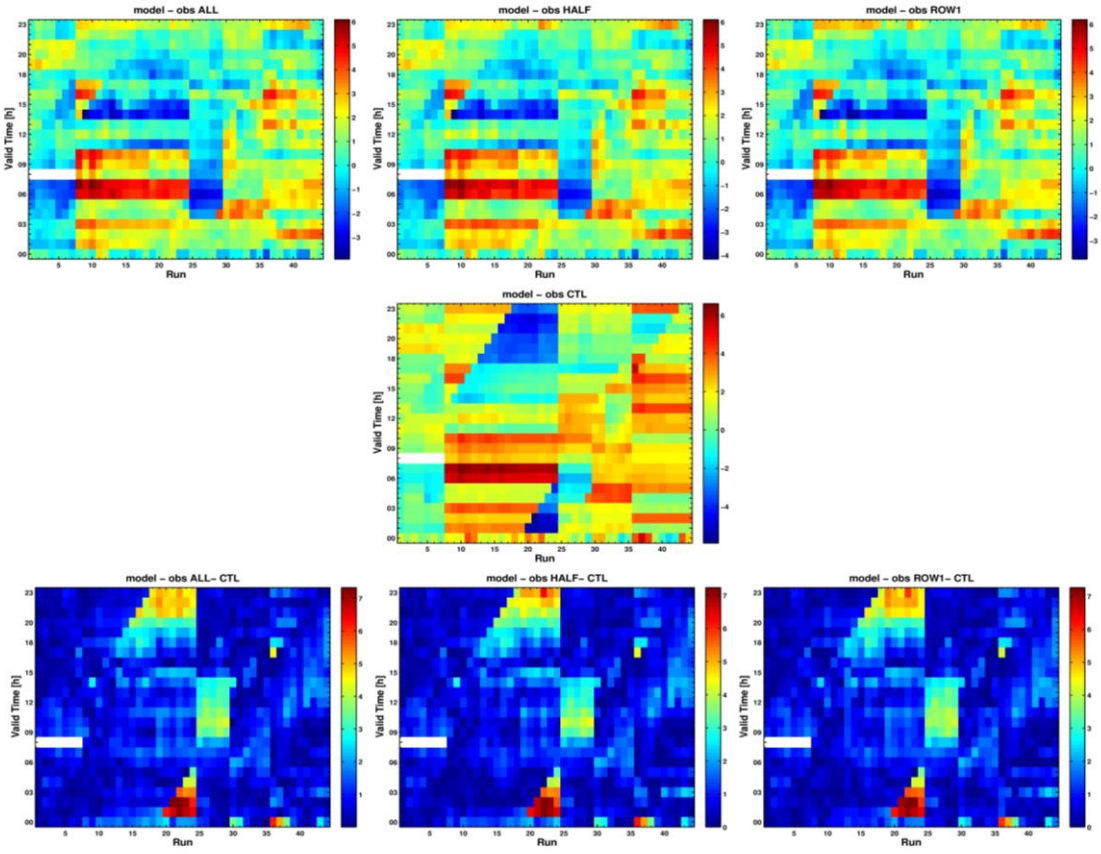


**Figure 13: Break down of the wind speed error (model minus observation) as a function of forecast run (x-axis) and valid time (y-axis) for experiments ALL (upper left), HALF (upper middle), ROW1 (upper right) and the CTL (middle) at M7. The differences of forecast errors of the experiments to the CTL are shown for experiments ALL (lower left), HALF (lower middle), ROW1 (lower right). Data void areas are left white.**

**Table 4: Same as Table II, but for all the test cases separately.**

| Aggregation | RMSE | Rank RMSE | CORR | Rank CORR | BIAS | Rank BIAS | Total Ranking |
|---|---|---|---|---|---|---|---|
| *Case 1: 29 May 11 UTC - 20 UTC* | | | | | | | |
| Row 1 | 0.811 | 8 | 0.910 | 1 | 0.708 | 8 | 17 |
| Row 2 | 0.746 | 5 | 0.811 | 4 | 0.175 | 5 | 14 |
| Row 3 | 0.764 | 6 | 0.799 | 7 | 0.159 | 4 | 17 |
| Row 4 | 0.766 | 7 | 0.797 | 8 | 0.103 | 3 | 18 |
| Row 5 | 0.684 | 3 | 0.803 | 6 | -0.084 | 2 | 11 |
| all | 0.639 | 1 | 0.824 | 3 | -0.041 | 1 | 5 |
| half | 0.722 | 4 | 0.807 | 5 | 0.177 | 6 | 15 |
| Rows 1&2 | 0.670 | 2 | 0.878 | 2 | 0.463 | 7 | 11 |
| *Case2: 19 July 13 UTC - 20 July 08 UTC* | | | | | | | |
| Row 1 | 1.459 | 8 | 0.669 | 7 | 0.572 | 8 | 23 |
| Row 2 | 1.435 | 7 | 0.655 | 8 | -0.064 | 3 | 18 |
| Row 3 | 1.380 | 5 | 0.680 | 5 | -0.056 | 2 | 12 |
| Row 4 | 1.382 | 6 | 0.688 | 4 | -0.106 | 4 | 14 |
| Row 5 | 1.363 | 3 | 0.705 | 2 | -0.295 | 6 | 11 |
| all | 1.300 | 1 | 0.729 | 1 | -0.326 | 7 | 9 |
| half | 1.373 | 4 | 0.680 | 6 | -0.043 | 1 | 11 |
| Rows 1&2 | 1.350 | 2 | 0.689 | 3 | 0.278 | 5 | 10 |
| *Case 3: 26 Aug. 00 UTC - 07 UTC* | | | | | | | |
| Row 1 | 0.790 | 2 | 0.509 | 1 | 0.269 | 2 | 5 |
| Row 2 | 1.019 | 5 | 0.355 | 8 | -0.598 | 4 | 17 |
| Row 3 | 1.071 | 7 | 0.408 | 6 | -0.707 | 7 | 20 |
| Row 4 | 1.023 | 6 | 0.398 | 7 | -0.634 | 5 | 18 |
| Row 5 | 1.086 | 8 | 0.425 | 4 | -0.764 | 8 | 20 |
| all | 1.004 | 4 | 0.471 | 2 | -0.697 | 6 | 12 |
| half | 0.961 | 3 | 0.411 | 5 | -0.547 | 3 | 11 |
| Rows 1&2 | 0.777 | 1 | 0.461 | 3 | -0.116 | 1 | 5 |
| *Case 4: 26 Aug. 13 UTC - 22 UTC* | | | | | | | |
| Row 1 | 0.906 | 2 | 0.581 | 1 | 0.468 | 3 | 6 |
| Row 2 | 1.026 | 6 | 0.387 | 8 | -0.529 | 4 | 18 |
| Row 3 | 1.026 | 7 | 0.434 | 7 | -0.585 | 6 | 20 |
| Row 4 | 1.006 | 5 | 0.456 | 6 | -0.562 | 5 | 16 |
| Row 5 | 1.075 | 8 | 0.493 | 3 | -0.704 | 8 | 19 |
| all | 0.990 | 4 | 0.574 | 2 | -0.654 | 7 | 13 |
| half | 0.946 | 3 | 0.468 | 5 | -0.464 | 2 | 10 |
| Rows 1&2 | 0.830 | 1 | 0.468 | 4 | 0.029 | 1 | 6 |
| *Case 5: 25 Oct. 16 UTC - 26 Oct. 03 UTC* | | | | | | | |
| Row 1 | 0.921 | 1 | 0.576 | 1 | -0.504 | 1 | 3 |
| Row 2 | 1.410 | 3 | 0.346 | 3 | -0.982 | 3 | 9 |
| Row 3 | 1.634 | 6 | 0.275 | 6 | -1.170 | 6 | 18 |
| Row 4 | 1.608 | 5 | 0.249 | 8 | -1.071 | 5 | 18 |
| Row 5 | 1.722 | 8 | 0.263 | 7 | -1.280 | 8 | 23 |
| all | 1.663 | 7 | 0.322 | 4 | -1.277 | 7 | 18 |
| half | 1.501 | 4 | 0.304 | 5 | -1.051 | 4 | 13 |
| Rows 1&2 | 1.106 | 2 | 0.482 | 2 | -0.715 | 2 | 6 |

## 3.6 Discussion and conclusion

This study is a first assessment of the assimilation of wind farm data, i.e., nacelle winds and yaw angles, which has been conducted with the WRF Four-Dimensional Data Assimilation (FDDA) system to improve shortest-term wind forecasts at the Danish offshore wind farm Horns Rev I. The challenges associated with these data, including wake effects on downwind turbines and disturbances of the measurements caused by the rotor blades, have been discussed. Since wind farm data are spatially

dense, there is need to produce a representative data set. This study focuses therefore on the evaluation of thinning strategies of wind farm data; these strategies include median nacelle winds of groups of turbines, such as the first, second, third, fourth and fifth upwind turbine row; all the turbines; the upwind half wind farm and the first two upwind rows together.

It has been shown that adding wind farm observations to already existing data used operationally to improve the initial conditions of a NWP model has the potential to produce more accurate low level wind predictions for wind energy applications both downstream of the wind farm and on the wind farm where data were assimilated. These results are relevant for the wind energy industry: Firstly, improving wind forecasts downstream of a wind farm is especially beneficial in areas with a high number of wind farms (e.g., the North Sea), where the assimilation of wind farm data from one farm has the potential to improve wind predictions for a nearby wind farm. Furthermore, since offshore wind farms are generally near the coast, assimilating their data has the potential to improve forecasts inland. Secondly, improving the accuracy of wind forecasts translates into a huge cost benefit for wind farm operators; since the power in the wind depends on the wind speed cubed, improved wind forecasts even for a short temporal scale and magnitude result in savings for Transmission System Operators and wind farm operators. Moreover, single poorly forecast events contribute heavily to the overall cost. In this study we evaluated thus test cases both separately, which gave an indication about the assimilation impact depending on weather situation, as well as through error metrics, which described the overall assimilation impact and include outliers in their performance (i.e., RMSE, bias, CRMSE and rank correlation). The latter helped assessing the overall benefit for wind energy applications, which was the aim in this study.

Initial computations of error metrics carried out with nacelle winds and wind measurements from M7 to find potential thinning strategies revealed that the median of the first two upwind turbine rows would have the lowest combined error metric. However, using the median wind speed of the whole wind farm performed best in the data assimilation experiments compared to the other thinning strategies. Since the model bias is positive, the most successful thinning strategy is the one that nudges the lowest wind speeds. The median of the whole wind farm was lower than the other strategies most of the time and thus the most successful. This implies that the best thinning strategy could be different when other NWP models are used or if the model behaviour at the location of interest is different from the one used in this study. Taking the median of the whole wind farm is very practical from an operational point of view, because it does not require a real-time pre-processing algorithm to detect which row or turbine is upwind. Note that down regulations, maintenance periods, and outages will decrease data quality and will have to be considered when assimilating wind farm data operationally. Moreover, transmission system operators usually convert the average wind forecast at hub height to one power forecast for the whole wind farm. When this wind forecast was initialized by assimilating the median of all turbines, which encompasses both wake affected and non-affected wind speeds and is thus lower, more realistic power estimates can be expected. True power distributions within a wind farm are also driven by wake affected and non-affected wind speeds. This was also concluded in [Cutler et al, 2011]. Wind direction measurements were not sensitive to the results; yaw angles constitute thus a potential data set that can be used successfully in data assimilation. This has the advantage that wind farm data can be used without additional (and usually expensive) tower measurements.
The assimilation impact lasted beyond 24 hours, which is far beyond the advection timescale. The impact beyond 2 hours was mainly due to the additional assimilation of upper air MADIS data, whereas the assimilation of wind farm data showed skill in improving CRMSE, RMSE and bias for the first 2 free forecast hours. This is within the timescale where the forecast improvement for wind energy applications is most valuable (section 3.1). The improvement of all these metrics together implies that the positive impact of wind farm data assimilation was not solely due to their advection downwind, but due the ability of FDDA to add predictive skill to the raw forecast; moreover, the fact that M7 and Horns Rev are both within the same radius of influence contributed further to the improvement of these metrics. An improved CRMSE suggests a reduction of phase errors. The rank correlation was mostly improved for lead times beyond 13 hours, which was not due to the assimilation of wind farm data. The difference in thinning strategies is most significant for the first 5 lead times. The assimilation impact depends on the time of the day, the forecast lead time and the weather situation. Even though all the test cases occurred during similar weather situations with unstable atmospheric conditions influenced by low pressure systems (section 3.4.2, Figure 8), different assimilation effects were encountered. It is

likely that the starting time of the simulations influenced the results as well. Due to the small sample size this effect was not quantifiable.
Even though most of the assimilation impact in the model domain is due to the additionally assimilated upper air observations, the additional impact of wind farm data is considerable. Sensitivity experiments indicated that the biggest impact is not necessarily close to the wind farm but can be a few hundred kilometres away, depending on the case (not shown). In areas sensitive to the assimilation procedure, different thinning techniques yielded different impacts in the wind field throughout the whole model domain. This shows that the biggest impact of the assimilation of wind farm observations is not necessarily at or downstream of the wind farm. Hence, assimilating wind farm data operationally will be promising for both wind energy predictions and weather predictions in general.
The restrictions for the case studies, although necessary for the conducted research, resulted in a limited number of cases and the results are thus likely to not be statistically significant. However, the results are relevant for the wind energy community and show a clear trend. For future studies we recommend thus a setup that allows case studies that yield more statistically robust results. This will make it necessary to re-define the “first upwind row”, which is straightforward in regularly shaped wind farms, but gets more complicated when the wind is not coming directly perpendicular towards
a regularly shaped wind farm edge. Moreover, since wakes depend besides wind speeds, atmospheric stability and turbulence intensity on wind farm layouts and size, the best thinning strategies for irregularly shaped and bigger wind farms might therefore be different and will have to be re–assessed.
The methods and issues concerning the assimilation of wind farm data on the example of FDDA are valid for any other data assimilation system alike. The benefit of assimilating wind farm observations in these other systems could lead to promising results as well. Likewise, the assimilation of observations in the boundary layer is a topic that still needs further research.
Since the field of wind energy is a commercial enterprise, wind farm operators are reluctant to provide their data. To assimilate wind farm data in an operational context, lobbying work will be necessary to make the data widely accessible. Hopefully this study is encouraging to advance initial steps, so that this new data set will be widely used in data assimilation in the future.

# 4. Data assimilation around the North Sea

The aim of this subtask is to analyse systematically the different variational data assimilation methodologies and schemes implemented in WRFvar. In contrast to section 3 where in particular the impact of wind farm observations and rather local meteorological observations has been studied, the domain is increased to enable the assimilation of meteorological observations spread over a larger area and, hence, to increase the impact on the forecasts.

## 4.1 Description of the test case

The WRF model domain used as a test bed to improve wind forecasts by assimilation of observational data covers Denmark, England, Ireland, Benelux and North Germany and can be seen in *Figure 18*. The domain is extended to the west for taking into account that most synoptic systems come from the west and that the observation coverage is dense over the British Isles.
The test period is April 2008. Each day at 00:00UTC the model is initialized. The different initial and boundary conditions are detailed in the section 4.2.

### 4.1.1 Assimilated meteorological observations

The observational data that are retrieved from ECMWF archives include land surface data, sea surface data and vertical soundings (radiosondes). Assimilated parameters are pressure, u,v wind speed, temperature and specific humidity. The data from synoptic land stations, ship sites and vertical soundings are available in different time intervals. The vertical sounding is usually taken every 6 hours, synop stations every 6 hours or hourly and ship observations are likely to be very irregular.
The spatial distribution of observational sites is very inhomogeneous (Figure 14). At 31 March 2008 439 observational sites are available (364 sites over land surface, 60 sites over sea surface, and 15 sites with vertical sounding). Figure 15 shows a T-logP diagram and wind at De Bilt, Netherlands, as an example for vertical sounding data.

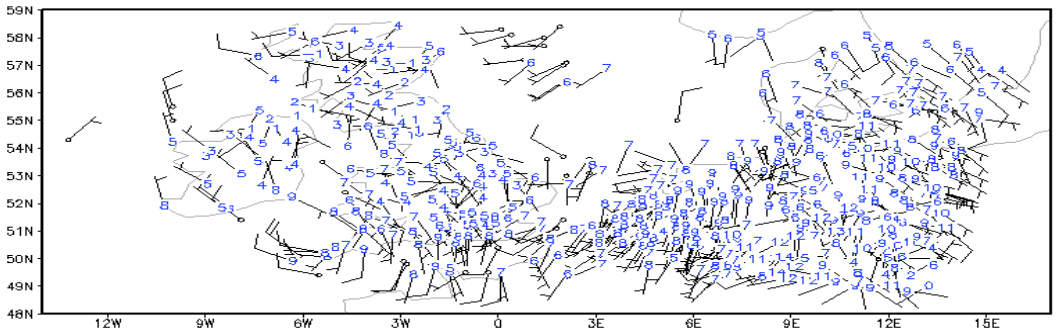


***Figure 14: Observational sites at 00 UTC 31 March 2008. The blue numbers show the temperature in centigrade, the barbs show the wind direction and velocity.***

The number of stations used for objective analysis and afterwards for FDDA or 3dVar is changing at each time step and vary between 410 to 500 for synop observations and 12 to 30 for vertical soundings.

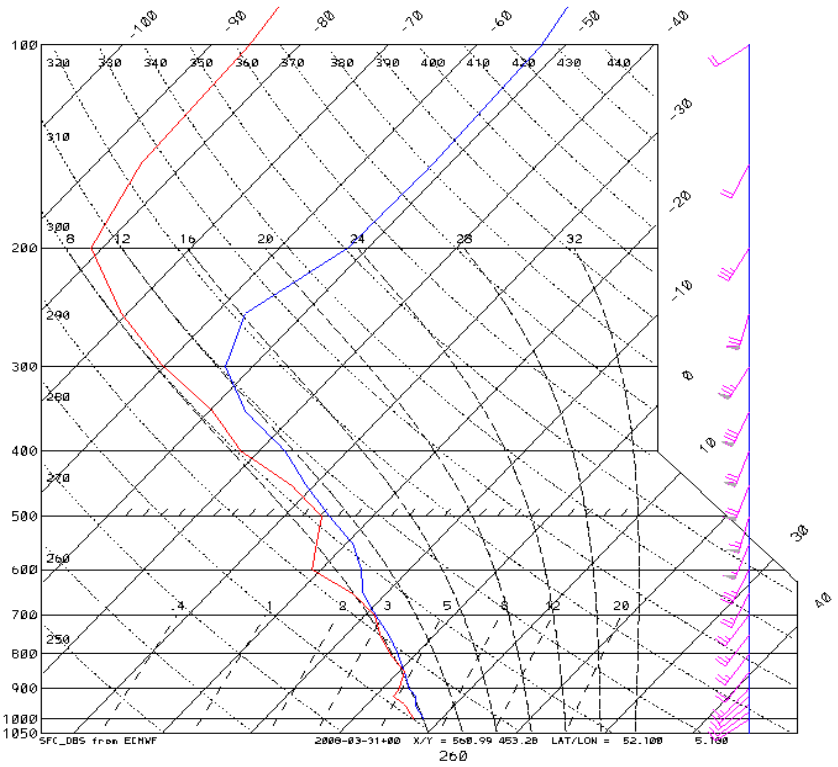


**Figure 15: T-logP diagram and wind at De Bilt, Netherlands (52.1°N, 5.1°E) at 00 UTC, 31 March 2008**

### 4.1.2 Initialization of the model

WRF is either initialized with NCEP or ECMWF forecast fields that are available on pressure levels. The horizontal resolution of NCEP is 0.5°x0.5° (~55 km) and T799 (~25 km) for ECMWF. The horizontal and vertical interpolation to WRF model grid points is performed first. In a second step the interpolation in time from three hourly to hourly is done. In order to include the impact of the observations at the initialization of the model, model runs (called experiments) with FDDA are started from an objective analysis. The algorithm of the objective analysis combines the first NCEP or ECMWF forecast (the first guess or background) with observations through the Cressman method (Cressman, 1959) and is performed in the WRFvar routine OBSGRID (Figure 1). A correction to the background field at a certain grid point is defined to be a weighted average of the observed increments within an "influence radius" R surrounding that grid point (Figure 16, left).

The impact of the objective analysis is presented in section 4.3.1. Note, that experiments with 3dVar are not initialized with the objective analysis but directly with data of the initializing model.

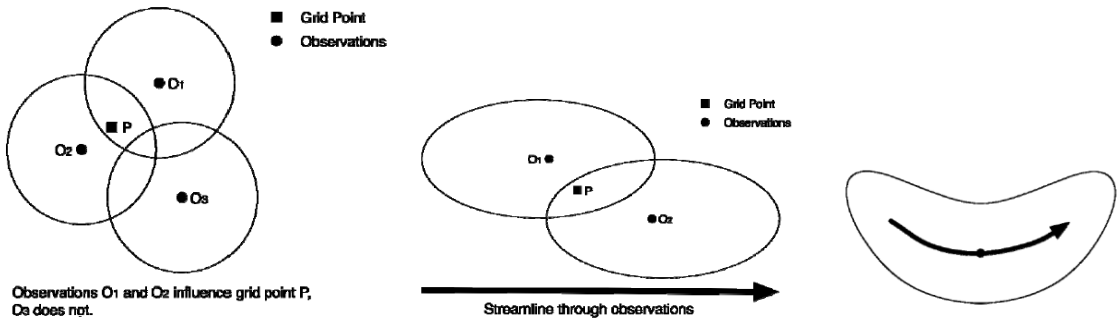


**Figure 16: Schematic diagram for standard Cressman scheme(left), the ellipse scheme from the standard Cressman scheme (middle) for straight-flow conditions, and the banana scheme from the standard Cressman scheme (right) for curved-flow conditions: circles are for observation sites, squares for grid points.**

### 4.1.3 Verification data

Independent verification of the WRF data assimilation results is done utilizing wind speed measurement at the FINO1 research platform in the North Sea. FINO1 is located 45 km northwest of the island Borkum (Figure 17). The top wind speed is measured at 100 m height with a cup anemometer. The averaging time is 10 minutes. WRF model levels in 75 m and 148 m above terrain are used to compute the model wind speed in 100 m height using linear interpolation.

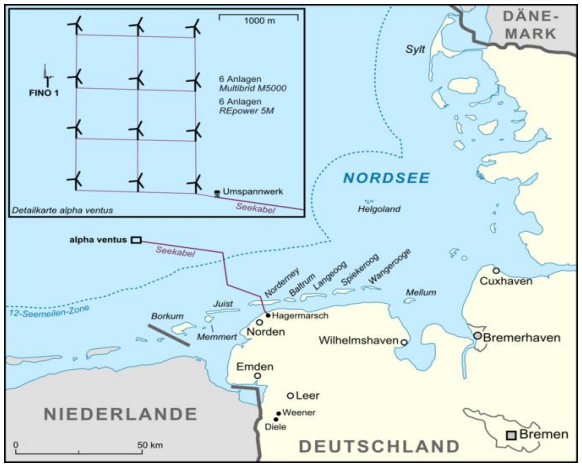


**Figure 17: Location of research platform FINO1 and the first German wind park in the North Sea 'alpha ventus' (Source: Wikipedia).**

Furthermore, 10 m wind speed and mean sea level pressure analyses of the COSMO-EU model provided by the German Weather Service (DWD) serve as verification to demonstrate the observation impact on experiments with data assimilation compared to experiments without data assimilation. It is assumed that the hourly COSMO-EU (DWD) analysis is very close to the real state of the atmosphere but one has to note that each model analysis contains the deficiencies of the model used for generating the analysis.

## 4.2 Model and experiment setup

Different sensitivity experiments are performed with WRFvar to find the optimal configuration for best wind forecast results. The following settings are common to all experiments:
The horizontal resolution is 10 km and no nesting is applied. 43 model levels are used and 9 of them are below 1 km. The lowest level is at 22 m. The integration time step is 60 sand data is archived every full hour.
Physical processes include cloud microphysics using WRF Single-Moment (WSM) 3-class simple ice scheme (Hong et al., 2004), longwave radiation using Rapid Radiative Transfer Model (RRTM) scheme (Mlawer et al., 1997), shortwave radiation using Dudhia scheme (Dudhia, 1989). The interval between each radiation physics call is 30 minutes.
All experiments are conducted with two different planetary boundary layer schemes: In the scheme labelled "pbl1" the surface layer physics is called "Monin-Obukhov" scheme. The boundary layer scheme is from Yonsei University (Hong et al, 2006) and the land surface module is based on 5-layer thermal diffusion (Dudhia, 1996).

In the experiment "pbl5" the schemes for the surface layer is Mellor-Yamada-Nakanishi-Niino scheme. The boundary layer scheme is Mellor-Yamada-Nakanishi-Niino 2.5-level TKE closure (Nakanishi and Niino, 2006) and the land surface module is unified Noah LSM (Ek et. al, 2003).

WRF downscaling experiments without data assimilation are used as reference for the data assimilation experiments. Both data assimilation schemes available in WRF have been tested, i.e. experiments with FDDA initialized from the objective analysis and 3dVar data assimilation. In the case of 3dVar the background error covariance is determined in two ways: i) standard background error

covariances are used which are provided within WRF for global use. ii) A different approach is to compute a domain dependent background error covariance that is determined by previous forecast runs for the same domain. The advantage is that in such a way obtained background error covariances are more specific to the model domain and initial data and thus lead to an improved usage for assimilated observations. However, the computational cost is comparably high to obtain these background error covariances because a forecast run for at least one month has to be carried out before. The 3dVar experiment with self-computed background error covariance is called 'non-standard' background error covariance.

All experiments are initialized with NCEP and ECMWF forecasts to analyse the impact of different initial conditions. Those forecasts also serve as boundary conditions during the model integration.

## 4.3 Results

### 4.3.1 Objective analysis increments

The impact of observational data in the objective analysis is illustrated in *Figure 18* for 10 m wind speed and wind speed in 925 hPa height. The analysis increment is defined as the difference between derived objective analysis and the first guess (background). The bias of analysis increments (bottom) shows the systematic influence of observations on the background. It can be seen that over extended areas the wind speed observations reduce the wind speed in the background field (negative increments) for surface and 925 hPa winds. The impact in 925 hPa height is limited to the sites with vertical soundings while the numerous synop observations have a very heterogeneous impact on the result of the objective analysis. The root mean square (RMS) of analysis increments also shows that vertical soundings have the largest impact but as they are sparse large areas are almost not influenced. The RMS of surface wind analysis increments demonstrates a rather local impact of synop observations, i.e. their information is almost not spread to surrounding areas.

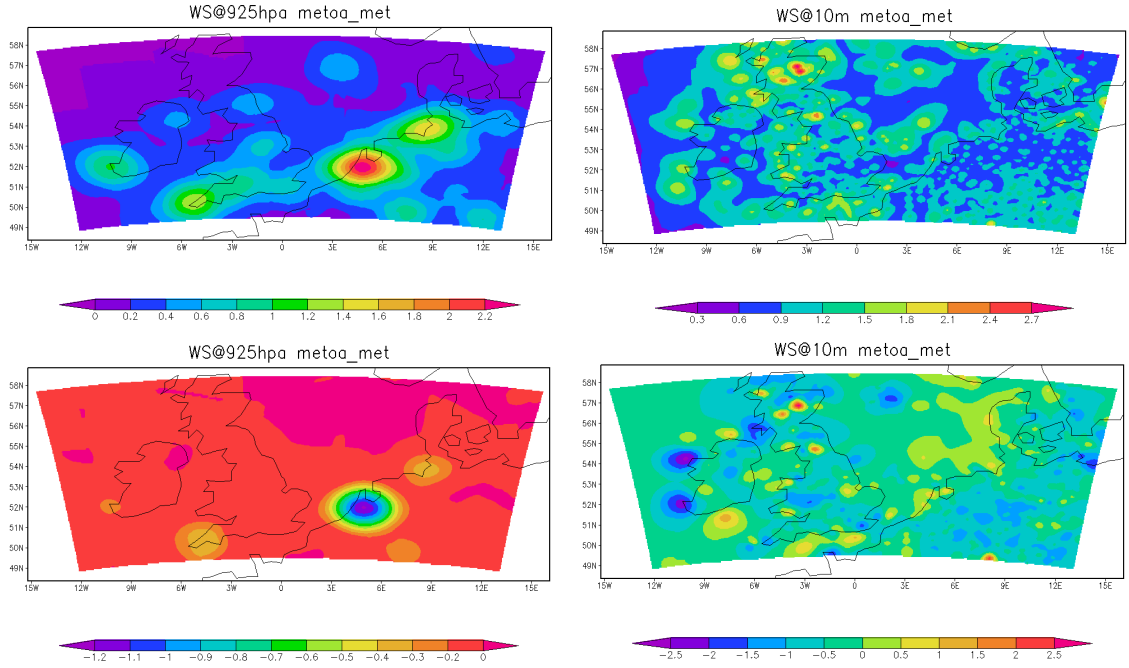


***Figure 18*: RMS (top) and bias (bottom) of objective analysis increments for 925 hPa wind speed (left) and 10 m wind speed (right) [m/s] for April 2008 using NCEP forecast as background fields.**

### 4.3.2 Impact of assimilation techniques

In this experiment the different impact of observations in 3dVar and FDDA is analysed. For each experiment the systematic and RMS difference between the WRF and the ECMWF 10 m wind speed serve as an indicator of how much the initial forecast has been changed during the assimilation (Figure 19). For the purpose of shortest-term wind power forecasting that relies on updates of wind power forecasts with observations, it is anticipated that the impact of observations is high, i.e. differences between WRF 10 m winds and initial ECMWF forecasts are high. In this respect the impact of observations in FDDA is stronger in terms of the RMS difference. Largest systematic and RMS differences exist in the North Sea and Northern UK and can be attributed to the 10 m wind speed objective analysis increments in *Figure 18* (right). For 3dVar assimilation with and without standard background error covariances the systematic difference is slightly positive while for FDDA the difference is mostly negative. This is in line with the negative systematic difference compared with FINO1 100 m wind speed (Figure 24, left) for FDDA. At FINO1 the 3dVar experiment shows a smaller systematic difference. On the other hand, the RMS difference between WRF data assimilation and FINO1 100m wind speeds is considerably smaller for FDDA compared to 3dVar (Figure 24, right). Almost no difference can be noted if standard (Figure 19, middle) or non-standard (Figure 19, bottom) background error covariances are used in 3dVar assimilation runs. The changes to the initializing ECMWF forecast (here: 10 m wind speed) are minor.

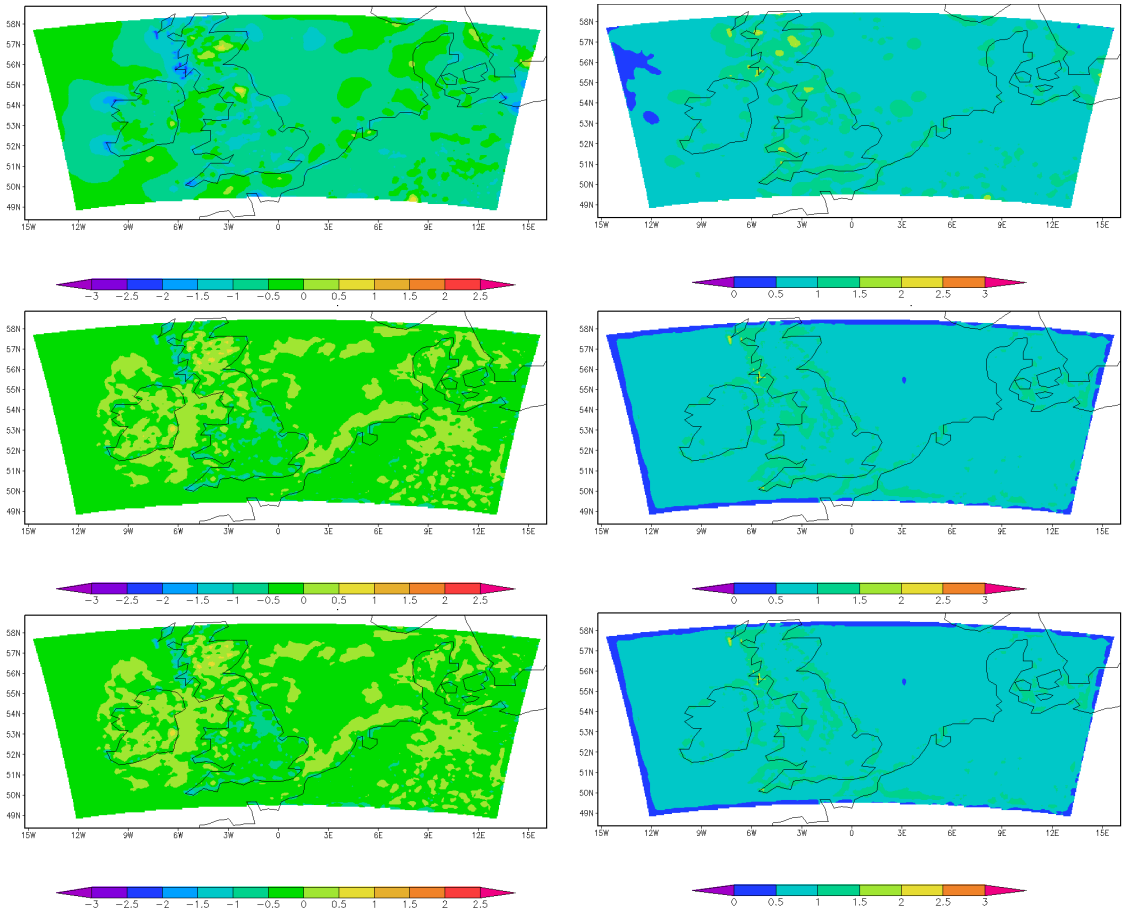

**Figure 19: 10 m wind speed [m/s] systematic (left) and RMS (right) difference between WRF with FDDA and initializing ECMWF forecasts (top) and between WRF with 3DVar and initializing ECMWF forecast (middle and bottom) for April 2008. PBL scheme 5 has been used. Non-standard observation error covariance has been used for the lower panels.**

### 4.3.3 Impact of initial conditions on data assimilation experiments

In contrast to section 4.3.2 the impact of data assimilation in WRF is verified in this section with analyses of the German Weather Service (DWD). Hence, it is possible to compare NCEP and ECMWF as initial conditions for the WRF experiments. 10 m wind speed and the mean sea level pressure are used as verification parameter. The results are presented for the PBL scheme 5 as the verification with FINO1 100 m wind speed shows clear advantages of PBL scheme 5 over PBL scheme 1 in terms of lower systematic and RMSE difference (Figure 24). Also see the discussion in section 4.3.4.

In Figure 20 (top panel) the systematic difference between the 10 m forecast wind speed of the initializing NWP model (NCEP (left) and ECMWF (right)) and DWD analysis is shown. It must be noted that the low resolution NWP data is interpolated (bilinear) to the WRF target grid (10 km). Compared to the DWD analysis NCEP short-term forecast have a negative wind speed bias for extended onshore areas (e.g. Great Britain, Ireland, Denmark, BeNeLux). In ECMWF forecasts this negative bias is only present for Ireland. For the North Sea NCEP winds have a stronger positive bias compared to DWD analysis than ECMWF. Both NWP models have in common that 10 m wind speeds at the North-West coast of Scotland and Ireland are strongly overestimated compared to DWD analysis. This difference occurs since in the low resolution of the global NWP models the rugged coast line of Scotland and Ireland with many small islands is very bad resolved leading to a surface roughness that is on average lower than in the DWD analysis. Conclusively, speeds in the NWP models are overestimated.

Downscaled NCEP and ECMWF forecasts reduce the systematic wind speed difference to the DWD analysis considerably for all areas. However, downscaled NCEP and ECMWF forecasts look very similar.

The application of FDDA lowers the 10 m wind speeds for NCEP and for ECMWF considerably compared to the DWD analysis. This trend to lower wind speeds due to FDDA is confirmed for 100 m winds at FINO1 (Figure 24, left).
The systematic wind speed difference between 3dVar results and DWD analysis is almost identical to the downscaling result (Figure 20), i.e. the assimilation of meteorological observations with 3dVar has almost no impact on the WRF result. Also when looking at the RMS wind speed difference between 3dVar result and DWD analysis (Figure 21) it must be stated that 3dVar results are not different from the pure downscaling run with WRF. However, FDDA has much lower onshore RMS differences compared to the downscaling and 3dVar results. The FDDA result with ECMWF data is slightly closer to the DWD analysis compared to NCEP initialisation.

In general, the RMS difference to 10 m DWD wind speed analysis shows that initialising ECMWF forecasts are closer to the DWD analysis. NCEP forecasts deviate in the North Sea and north-west of Ireland considerably more from DWD than ECMWF. The RMS difference exceeds 2 m/s in certain areas (Figure 21, top). The higher skill of ECMWF forecasts is confirmed after the downscaling with WRF, i.e. the 10 m wind speeds from WRF show smaller RMS differences to DWD than downscaled NCEP forecasts.

In terms of mean sea level pressure ECMWF initial conditions are closer to the DWD analysis with respect to systematic and RMS difference than NCEP forecasts (Figure 22, Figure 23). After downscaling of NCEP and ECMWF the mean sea level pressure difference has increased for initialisations from both NWP models. For onshore regions the mean sea level pressure has dropped while it increased for offshore areas.
FDDA further decreases the mean sea level pressure in Middle Germany but lowers on the other hand the RMS difference for all areas. It is obvious that also with FDDA the mean sea level pressure is closer to the DWD analysis when WRF is initialised with ECMWF forecasts.

Compared to 10 m wind speeds the impact of 3dVar is strongly positive for mean sea level pressure. The much lower RMS difference shows that 3dVar performs much better than FDDA (Figure 23). A small advantage of non-standard background error covariances over standard background error covariances can be noted leading to lower RMS differences. The initialisation with ECMWF is slightly outperforming NCEP. However, the impact of 3dVar is far more beneficial for NCEP than ECMWF since the high RMS difference between NCEP initial conditions and DWD analysis is reduced much more than for ECMWF.

Initial conditions

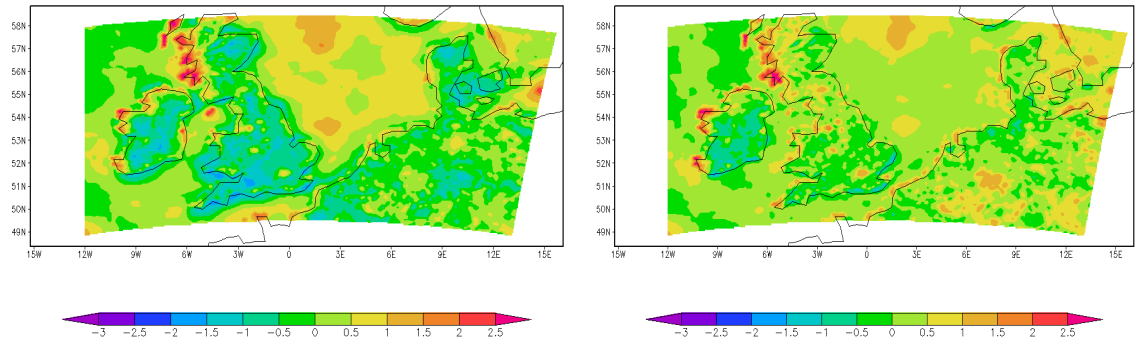

Downscaling

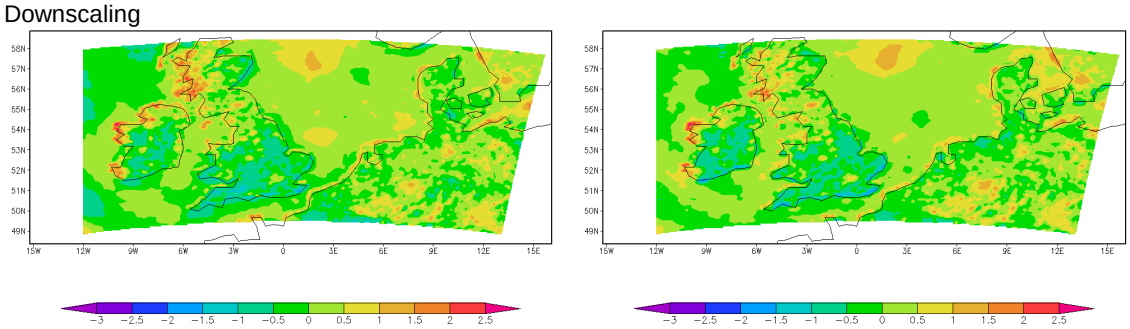

FDDA

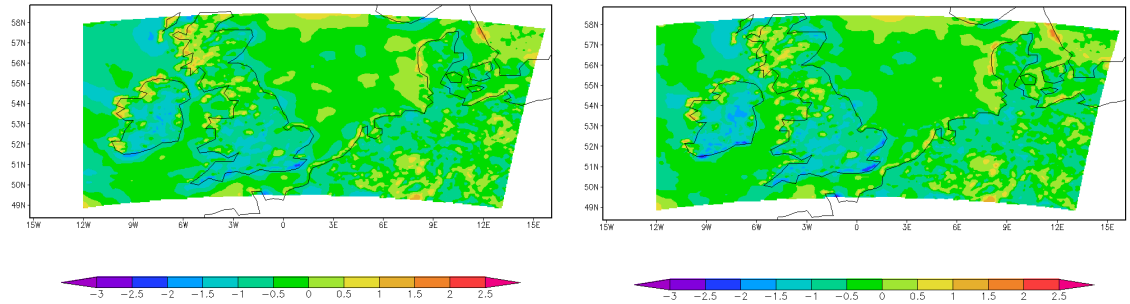

3dVar (standard background error covariance)

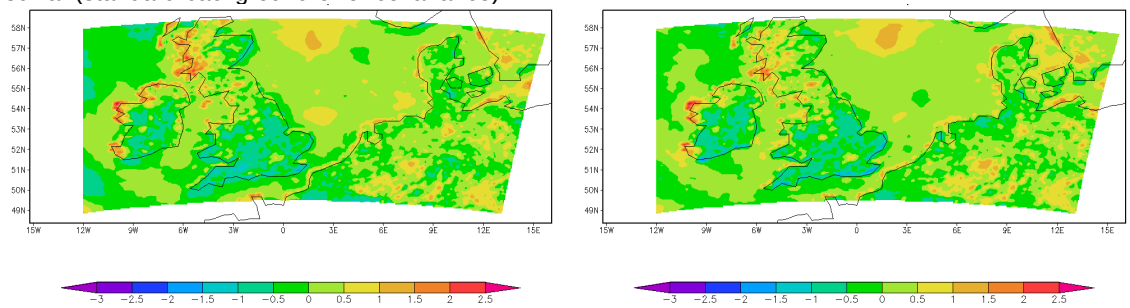

3dVar (non-standard background error covariance)

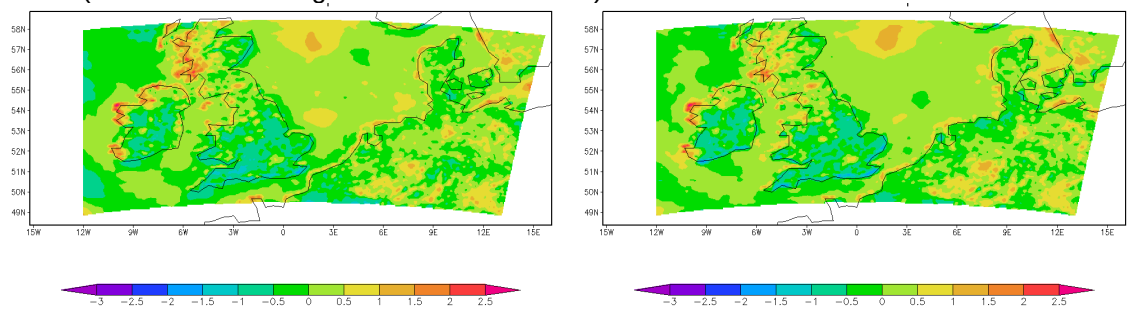

**Figure 20: 10 m wind speed [m/s] systematic difference between initializing forecast and DWD analysis, WRF downscaling experiment and DWD analysis, WRF FDDA experiment and DWD analysis, WRF 3dVar with and without standard error covariance and DWD analysis. Left for NCEP and right for ECMWF forecasts as initial conditions for April 2008 with PBL scheme 5.**

Initial conditions

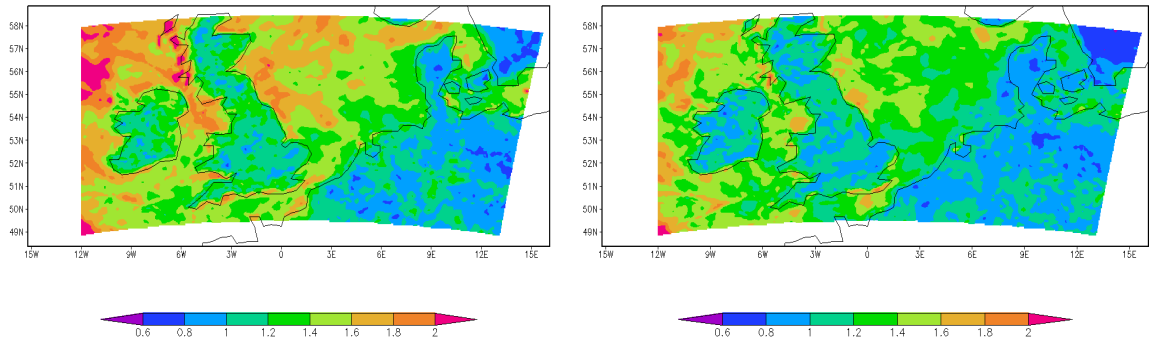

Downscaling

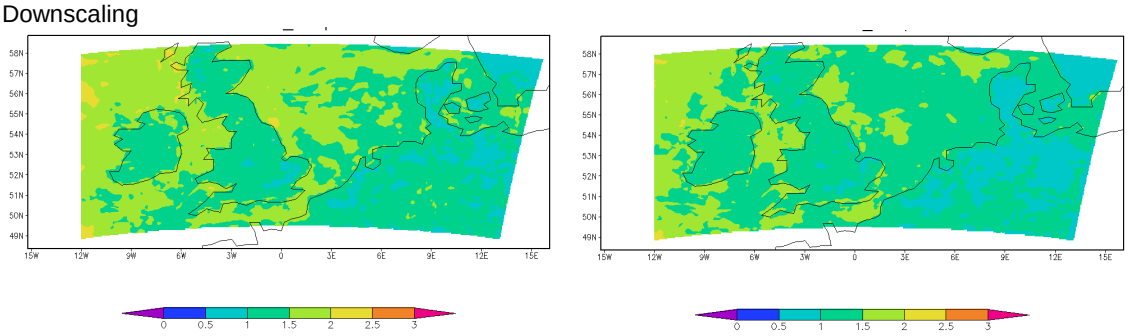

FDDA

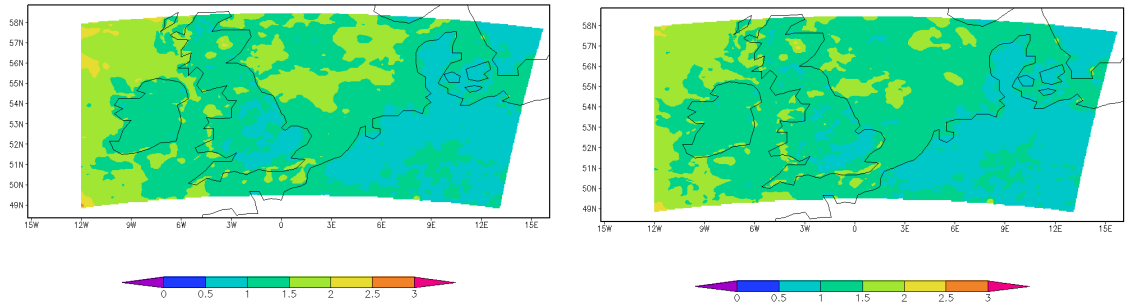

3dVar (standard background error covariance)

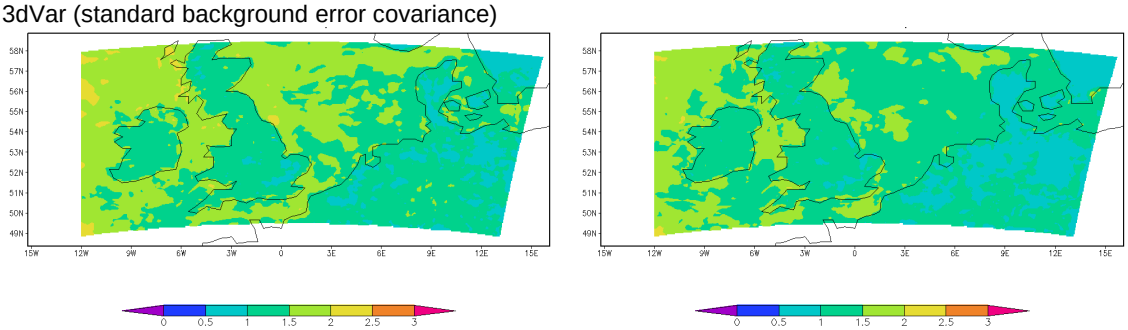

3dVar (non-standard background error covariance)

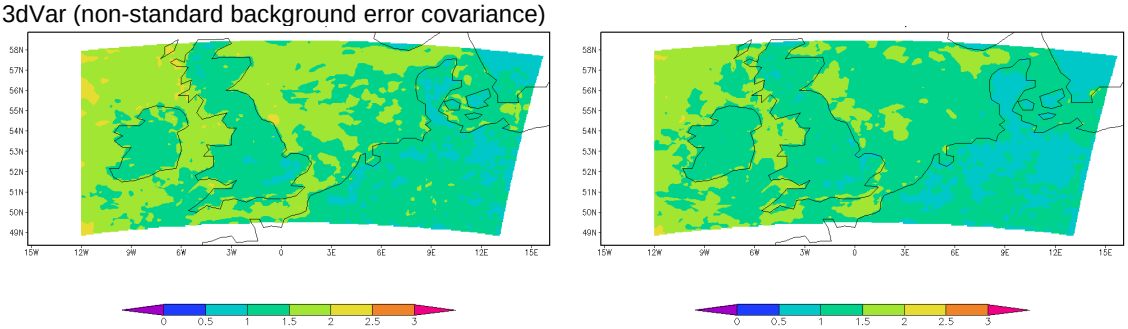

**Figure 21: As Figure 20, but 10 m wind speed [m/s] RMS difference.**

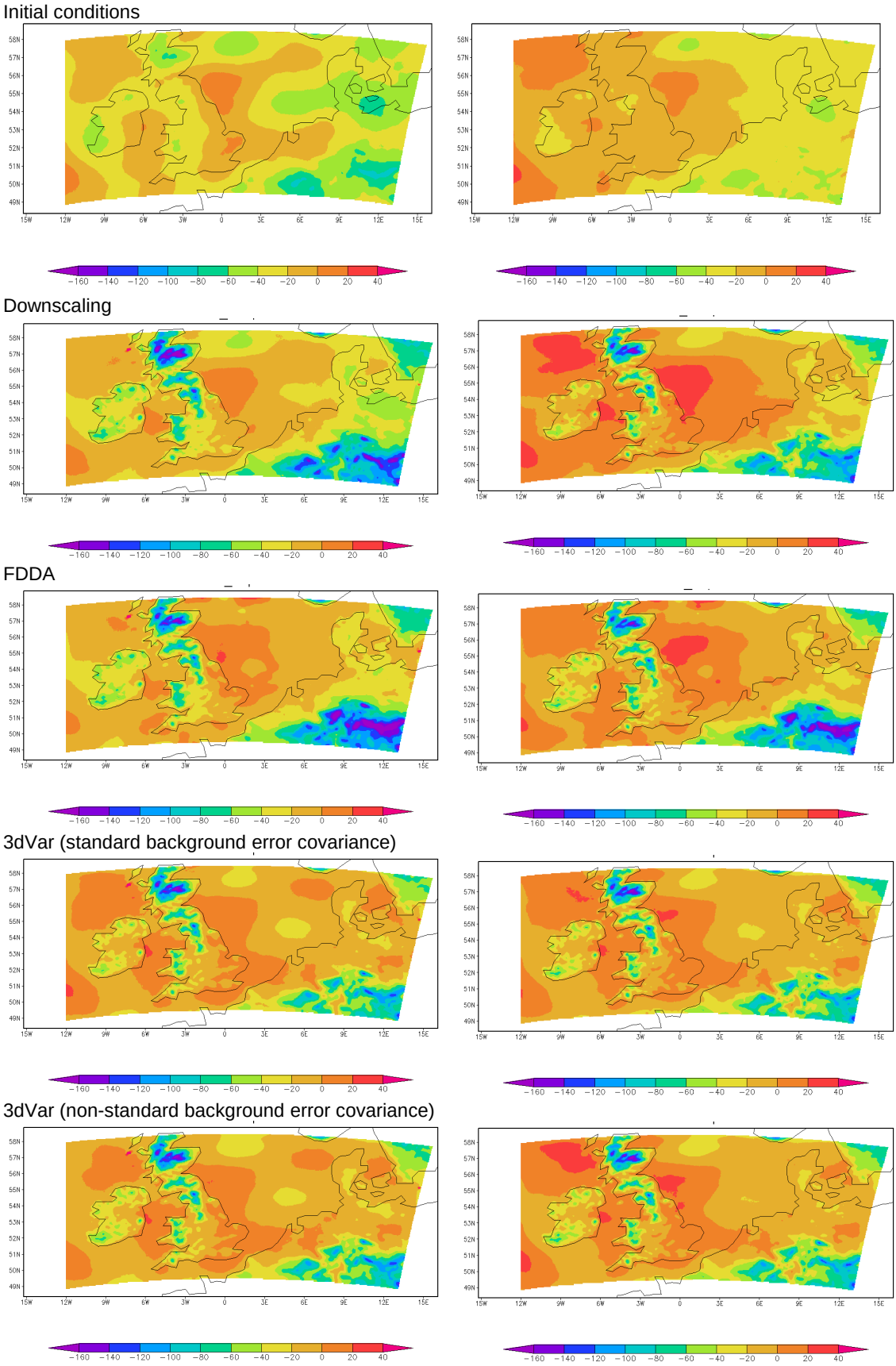


**Figure 22: Mean sea level pressure [Pa] systematic difference between initializing forecast and DWD analysis, WRF downscaling experiment and DWD analysis, WRF FDDA experiment and DWD analysis, WRF 3dVar with/without standard error covariance and DWD analysis. Left for NCEP and right for ECMWF forecasts as initial conditions for April 2008 with PBL scheme 5.**

Initial conditions

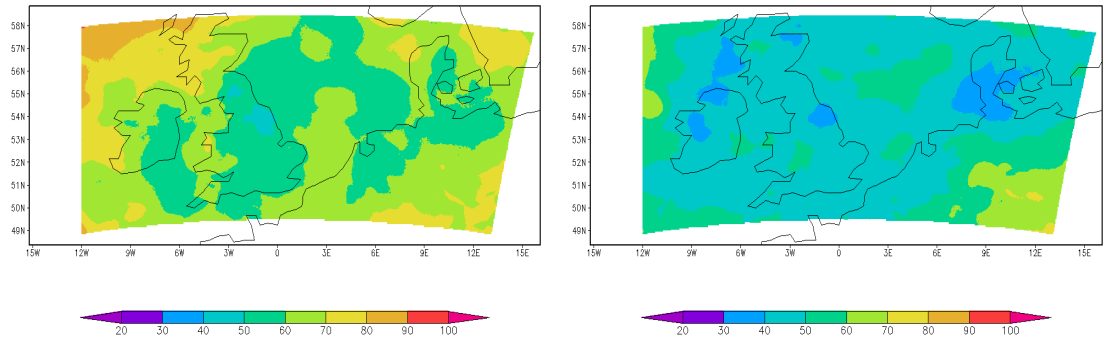

Downscaling

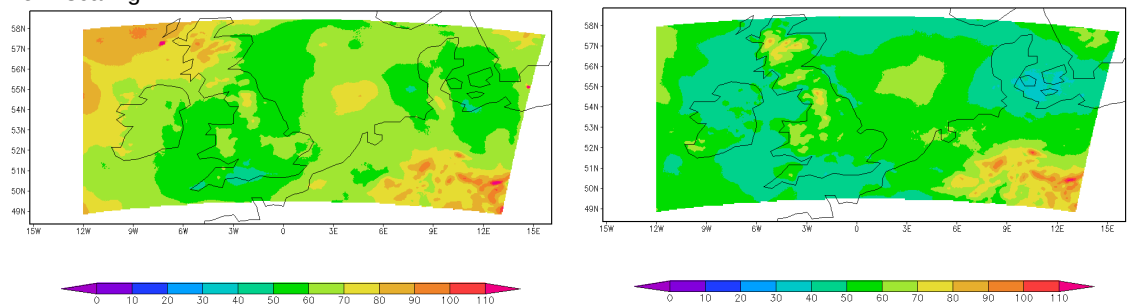

FDDA

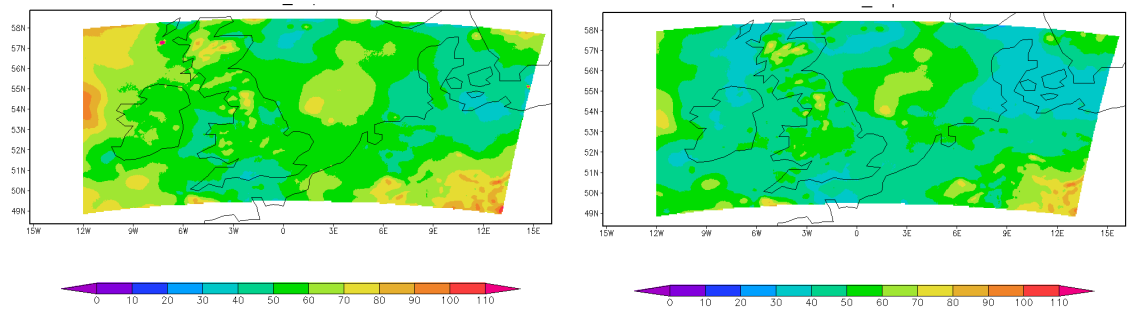

3dVar (standard background error covariance)

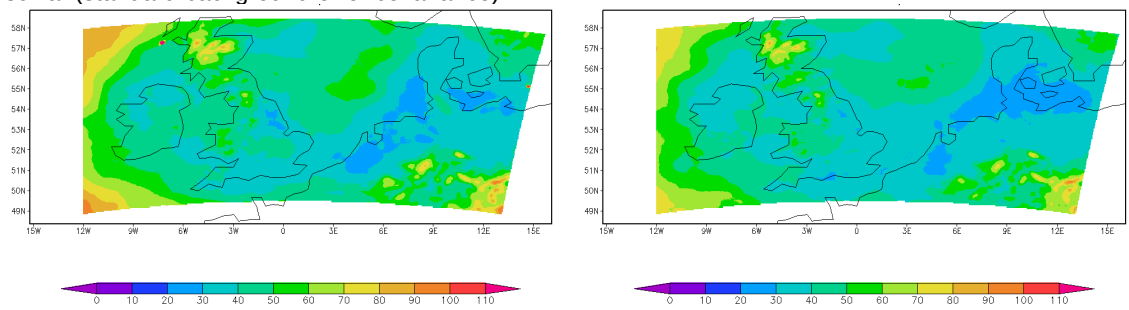

3dVar (non-standard background error covariance)

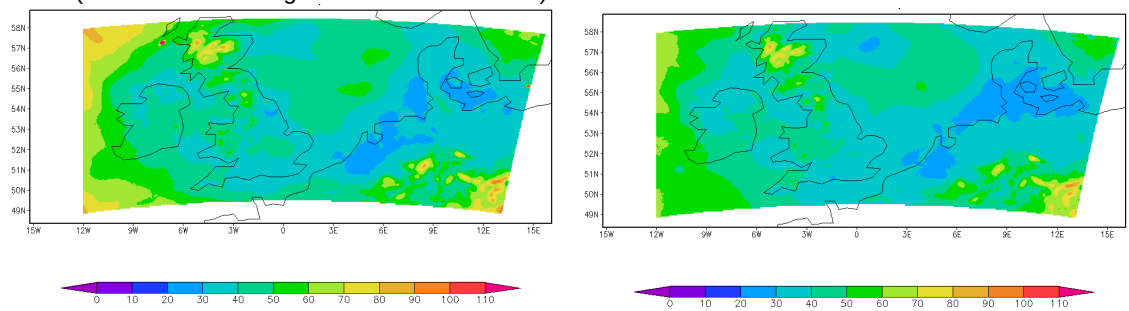

**Figure 23: As Figure 22 but for mean sea level pressure [Pa] RMS difference.**

### 4.3.4 Verification with FINO1

Figure 24 summarizes the verification of the conducted experiments with observed FINO1 100 m wind speeds for April 2008. In general, WRF simulations with PBL scheme 5 (see section 4.2) perform much better in terms of systematic and RMS difference. The bias of -0.5 m/s between initialising NWP model and FINO1 is best reduced with pure downscaling experiments and almost unchanged in FDDA experiments. On the other hand, FDDA runs decrease the RMSE difference most effectively compared to 3dVar (non-standard background error covariance) and pure downscaling runs. For ECMWF the RMSE decreases from 1.8 m/s (ECMWF forecast) to 1.5 m/s (ECMWF FDDA) and from 2.05 m/s for NCEP forecast to 1.65 m/s (NCEP FDDA). The RMSE is only slightly reduced by downscaling alone compared to the initialising forecast. However, it is questionable if in a real-time environment similar improvements can be gained. It must be noted, that the UNIOL experiments do not contain a “free” forecast run, i.e. at each time step observations have been assimilated and no forward integration was done. Furthermore the delivery time for ECMWF/NCEP forecasts to initialise WRF might be up to 12 hours later than the base time. Those considerations have not been taken into account in the current study.

The initialisation with ECMWF clearly outperforms NCEP initialisation. However, the initialisation with the NCEP analyses (NCEP FNL) leads to better RMSE results than ECMWF forecasts, but it must be kept in mind that a WRF forecast run cannot be performed with analyses.

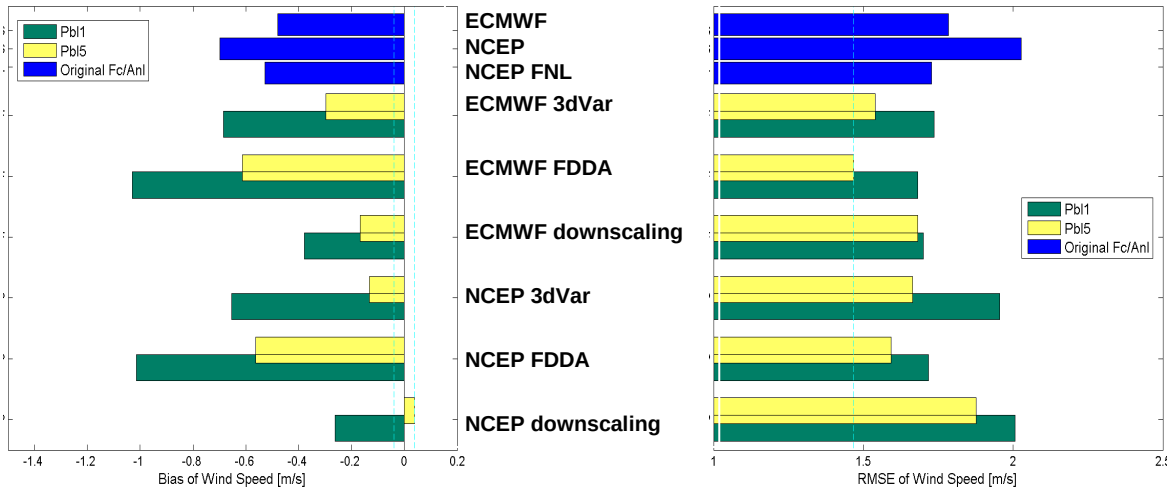


**Figure 24: Systematic differences (left) and RMSE (right) of 100 m wind speed for various WRF experiments (see text for details) verified with FINO1 observed wind speed for April 2008.**

# 5. Conclusion

In Task 4.2 “Data assimilation based on observations and detection of large forecast deviations due to extreme events” the partners University Oldenburg and DTU.RISOE investigated the potential of data assimilation with the mesoscale WRF (Weather and Research Forecasting) model in two different case studies.

DTU.RISOE utilizes the offshore wind park Horns Rev I as a test bed to assimilate wind speeds from up to 80 nacelle anemometers into WRF. WRF has been initialized with NCEP analysis and a 1-way nesting is done for the inner domains with 30 km and finally 10 km resolution. The inner domain has a size of 450 km x 650 km. Five test cases with varying length in May, July, August and October 2005 have been computed. The FDDA assimilation impact lasted beyond 24 hours, which is far beyond the advection timescale. The impact beyond 2 hours was mainly due to the additional assimilation of upper air MADIS data, whereas the assimilation of wind farm data showed skill in improving CRMSE, RMSE and bias for the first 2 free forecast hours. This is within the timescale where the forecast improvement for wind energy applications is most valuable (section 3.1).

The results clearly indicate that FDDA is improving the forecasts, but only for a few hours. The effect is advected out downstream and does not affect the wind farm anymore after about 2 hours. It has been found that almost no difference exists if wind speeds of only one turbine or of 80 turbines are assimilated. Actually, the median wind speed of the 80 nacelle anemometers leads to the best results.

UNIOL has applied FDDA and 3dVar for a domain of 1000 km x 1600 km size and a horizontal resolution of 10 km. About 470 synop, buoys and air craft reports plus about 20 vertical soundings have been assimilated per hour during the study period of 1-30 April 2008. As first guess fields the short-range forecasts of NCEP and ECMWF have been used, respectively.
It was found that with FDDA the observations have a stronger impact, because RMS increments (new analysis minus first guess) are slightly higher than for 3dVar. However, FDDA lowers in contrast to 3dVar the mean 10 m wind speed (bias) compared to the first guess.

The experiments show that ECMWF initial conditions (here 10 m wind speed and mean sea level pressure) are much closer to the verifying DWD analysis than NCEP initial conditions. This superiority of ECMWF forecasts remains when the forecast are downscaled with WRF. The application of FDDA or 3dVar reduces the difference in initialisation (NCEP or ECMWF) almost completely. It can be noted that initialisation with NCEP profits slightly less from 3dVar than ECMWF.

Assuming that the DWD analysis is very close to the real state of the atmosphere, the result with 3dVar is better, i.e. closer to the DWD analysis, for mean sea level pressure than FDDA. On the other hand, slight advantages for FDDA can be noted for the 10 m wind compared to 3dVar. The verification with FINO1 100 m wind speeds shows clearly that FDDA for ECMWF and NCEP matches the measurement better than 3dVar. However, with 3dVar a lower systematic error occurs. The comparison with FINO1 also shows that pure downscaling and data assimilation improves shortest-term forecast compared to original NCEP and ECMWF forecasts. In the best case, WRF FDDA lowered the initial ECMWF RMSE from 1.75 m/s to 1.45 m/s. However, it has been shown that the selection of the appropriate PBL scheme in WRF is essential to obtain such positive results.

In general, when assessing the often small improvement by data assimilation of observations, one has to bear in mind that a few observations are not able to change the entire flow in the model domain. The model has (in the case of UNIOL) about 700.000 grid boxes and consequently a huge “inertia” that is very hard to be changed by a couple of observations. The very efficient data assimilation at NWP centers is mainly based on the assimilation of satellite based observations that are available with much higher spatial density.
The use of high spatial resolved satellite data (e.g. 10 m wind speeds from the Advanced Synthetic Aperature Radar (ASAR) onboard ENVISAT with spatial resolutions down to 150 m) can be envisaged over ocean to assimilate high density observations into mesoscale models. Since approaching fronts can be observed with ASAR, it should be possible to improve the timing of fronts for shortest term wind power forecasts. Data from ground based rain radar are already assimilated in the COSMO-DE model

of the German Weather Service for better prediction of heavy rainfall (Stephan et al., 2008). Lindskog et al, 2004 assimilated radial wind speeds of a Doppler Radar to the HIRLAM model and showed improved forecast skills. Within the coming years it will be possible to subdivide radial wind speeds in their components through the superposition of Doppler Radar images measured by different instruments. It will be worthwhile to assimilate those new observation techniques into WRF for future study cases.

## References

Antoniou I, Pedersen TF. Nacelle anemometry on a 1 MW wind turbine. *Technical Report Risø-R-941(EN)*, Risø DTU 1997.

Barker, D. M., W. Huang, Y.-R. Guo, et al. 2004: A three-dimensional variational data assimilation system for MM5: Implementation and initial results. Monthly Weather Review, 132: 897-914.

Barthelmie RJ, Pryor SC, Frandsen ST, Hansen KS, Schepers JG, Rados K, Schlez W, Neubert A, Jensen LE, Neckelmann S. Quantifying the impact of wind turbine wakes on power output at offshore wind farms. *J. Atmos. Oceanic Technol.* 2010; **27**:1302–1317, doi:10.1175/2010JTECHA1398.1.

Barthelmie RJ, Jensen LE. Evaluation of wind farm efficiency and wind turbine wakes at the Nysted offshore wind farm. *Wind Energy* 2010; **13**:573–586, doi:10.1002/we.408.

Beyer H.G., T. Pahlke, W. Schmidt, H.-P. Waldl and U. de Witt (1994). Wake effects in a linear wind farm. J. Wind Eng. Ind. Aerodyn. 51, 303-318.

Botterud A, Wang J, Monteiro C, Miranda V. Wind power forecasting and electricity market operations. *32nd IAEE International Conference*, San Francisco, U.S.A., 2009.

Botterud A, Wang J, Miranda V, Bessa RJ. Wind power forecasting in U.S. electricity markets. *The Electricity Journal* 2010; **23**:71–82.

Cheng WY, Liu Y, Liu Y, Mahoney B, Politovich M, Warner TT, Parks K, Himelic J. Improving the 0-6 hour wind forecast through wind farm data assimilation in the NCAR/ATEC WRF-ARW RTFDDA. *Poster at the 12th Annual WRF Users' Workshop*, Boulder, U.S.A., 2011.

Christiansen MB, Hasager CB. Wake effects of large offshore wind farms identified from satellite SAR. *Remote Sensing of Environment* 2005; **98**:251 – 268, doi:10.1016/j.rse.2005.07.009.

Cressman, G. P., 1959: An operational objective analysis system. Monthly Weather Review. 87(10): 367-374.

Cutler NJ, Outhred HR, MacGill IF. Using nacelle-based wind speed observations to improve power curve modeling for wind power forecasting. *Wind Energy* 2011; doi:10.1002/we.465.

Daley R. *Atmospheric data analysis*. Cambridge University Press, 1991.

Delle Monache L, Glascoe L, J L, Mirocha J, Simspon M, Singer M. Ensemble-based data assimilation for wind energy predictions. *Fifth International Symposium on Computational Wind Engineering*, North Carolina, U.S.A., 2010.

Delle Monache L, Nipen T, Liu Y, Roux G, Stull R. Kalman filter and analog schemes to post-process numerical weather predictions. *Mon. Wea. Rev.* 2011; **139**:3554–3570, doi:10.1175/2011MWR3653.1.

*Dudhia, J., 1989: Numerical study of convection observed during the winter monsoon experiment using a mesoscale two-dimensional model. J. Atmos. Sci., 46, 3077–3107.*

*Dudhia, J, 1996: A multi-layer soil temperature model for MM5. Sixth Annual PSU/NCAR Mesoscale Model Users' Workshop, Boulder CO, July 1996, 49-50.*

*Ek, M.B., K. E. Mitchell, Y. Lin, E. Rogers, P. Grunmann, V. Koren, G. Gayno, J. D. Tarpley, 2003: Implementation of Noah land surface model advances in the National Centers for Environmental Prediction operational mesoscale Eta model. J. Geophys. Res. 108, 8851-8867*

Frandsen S, Sørensen J, Mikkelsen R, Pedersen T, Antoniou I, Hansen K. The generics of wind turbine nacelle anemometry. *European Wind Energy Conference*, Marseille, France, 2009.

Hong, Song-You, Jimy Dudhia, Shu-Hua Chen, 2004: A Revised Approach to Ice Microphysical Processes for the Bulk Parameterization of Clouds and Precipitation. Mon. Wea. Rev., 132, 103–120.

*Hong, Song-You, Yign Noh, Jimy Dudhia, 2006: A New Vertical Diffusion Package with an Explicit Treatment of Entrainment Processes. Mon. Wea. Rev., 134, 2318–2341.*

Ide K., P. Courtier, M. Ghil, et al., 1997: Unified notation for data assimilation: Operational, sequential & variational. J. Met. Soc. Japan. 75: 181-189.

Larson, K. A., K. Westrick, 2006: Short-term Wind Forecasting Using Off-site Observations, Wind Energy, **9**, 55-62.

Lazarus SM, Splitt ME, Lueken MD, Ramachandran R, Li X, Movva S, Graves SJ, Zavodsky BT. Evaluation of data reduction algorithms for real-time analysis. *Wea. Forecasting* 2010; **25**:837–851, doi:10.1175/2010WAF2222296.1.

Lindskog, M., K. Salonen, H. Järvinen, D. B. Michelson, 2004: Doppler Radar Wind Data Assimilation with HIRLAM 3DVAR. Mon. Wea. Rev., 132, 1081–1092

Liu Y, Warner T, Liu Y, Vincent C, Wu W, Mahoney B, Swerdlin S, Parks K, Boehnert J. Simultaneous nested modeling from the synoptic scale to the LES scale for wind energy applications. *Journal of Wind Engineering and Industrial Aerodynamics* 2011; **99**:308 – 319, doi:10.1016/j.jweia.2011.01.013.

Liu Y, Cheng W, Liu Y, Wiener G, Frehlich R, Mahoney W, Warner T, Himelic J, Parks K, Early S. Impact of assimilating met-tower, turbine nacelle anemometer and other intensified wind farm observation systems on 0 – 12h wind energy prediction using the NCAR WRF-RTFDDA model. *10th EMS Annual Meeting and 8th ECAC*, Zuerich, Switzerland, 2010.

Marquis M, Wilczak J, Ahlstrom M, Sharp J, Stern A, Smith JC, Calvert S. Forecasting the wind to reach significant penetration levels of wind energy. *Bull. Amer. Meteor. Soc.* 2011; **92**:1159–1171, doi:10.1175/2011BAMS3033.1.

Mesoscale & Microscale Meteorology Division, NCAR. User's Guide of Advanced Research WRF version 3. April 2009.

Mlawer, E.J., S.J. Taubman, P.D. Brown, M.J. Iacono and S.A. Clough: RRTM, a validated correlated-k model for the longwave. J. Geophys. Res., 102, 16,663-16,682, 1997.

Nakanishi, M., H. Niino, 2006: An Improved Mellor–Yamada Level-3 Model: Its Numerical Stability and Application to a Regional Prediction of Advection Fog. Boundary-Layer Meteorology 119:2, 397-407

Ochotta T, Gebhardt C, Saupe D,WergenW. Adaptive thinning of atmospheric observations in data assimilation with vector quantization and filtering methods. *Quarterly Journal of the Royal Meteorological Society* 2005; **131**:3427–3437, doi:10.1256/qj.05.94.

Pedersen T. Characterisation and classification of RISØ p2546 cup anemometer. *Technical Report*, Risø-R-1364(ed.2), Risø DTU 2004.

Pedersen TF, Gottschall J, Kristoffersen JR, Dahlberg JA. Yawing and performance of an offshore wind farm. *European Wind Energy Conference*, Warsaw, Poland, 2010.

Peña A.D., 2009: Sensing the wind profile. ISBN: 978-87-550-3709-0, Risø-PhD-45(en), DTU Wind Energy, Denmark

Skamarock WC, Klemp JB, Dudhia J, Gill DO, Barker MG Duda, Huang XY, DM, Wang W, Powers JG. A description of the advanced research WRF version 3. *Technical Report*, NCAR Tech Notes-475+STR 2008.

Smaili A, Masson C. On the rotor effects upon nacelle anemometry for wind turbines. *Wind*

*Engineering* 2004; **28**:695714, doi:10.1260/0309524043729958.

Stauffer D. R., and N. L. Seaman, 1990: Use of four-dimensional data assimilation in a limited area mesoscale model. Part I: Experiments with synoptic-scale data. Mon. Wea. Rev., 118, 1250-1277.

Stauffer D. R., and N. L. Seaman, 1994: Multi-scale four-dimensional data assimilation. J. Appl. Meteor., 33, 416-434.

Stephan K., S. Klink, C. Schraff, 2008: Assimilation of radar derived rain rates into the convective scale model COSMO-DE at DWD. Q.J.R.Meteorol.Soc. 134, 1315-1326

Taylor KE. Summarizing multiple aspects of model performance in a single diagram. *J. Geophys. Res.* 2001; **106**:7183–7192, doi:10.1029/2000JD900719.

Wessel, A., J. Dobschinski, B. Lange, 2009: Integration of offsite wind speed measurements in shortest-term wind power prediction systems. Proceedings of the 8th International Workshop on Large-Scale Integration of Wind Power into Power Systems, Bremen, 2009

Wilks DS. *Statistical methods in the atmospheric sciences*, *International Geophysics Series*, vol. 91. 2nd edn., Academic Press, 2006.

WRF3, WRF-ARW Version 3 Modeling System User's Guide. Mesoscale & Microscale Meteorology Division, National Center for Atmospheric Research, Boulder, USA 2010

Zahle F, Sørensen N.N., 2011: Characterization of the unsteady flow in the nacelle region of a modern wind turbine. Wind Energy, 14, 271–283, doi:10.1002/we.418.

Zupanski D, Paquin K, Kelly R, Nelson S, Zupanski M, Jankov I, Mallapragada P. Applications of data assimilation methodologies in wind power forecasting. *EGU General Assembly*, Vienne, Austria, 2010.